Cell Metabolism

Article

Hepatic BMAL1 and HIF1α regulate a time-dependent hypoxic response and prevent hepatopulmonary-like syndrome

Graphical abstract

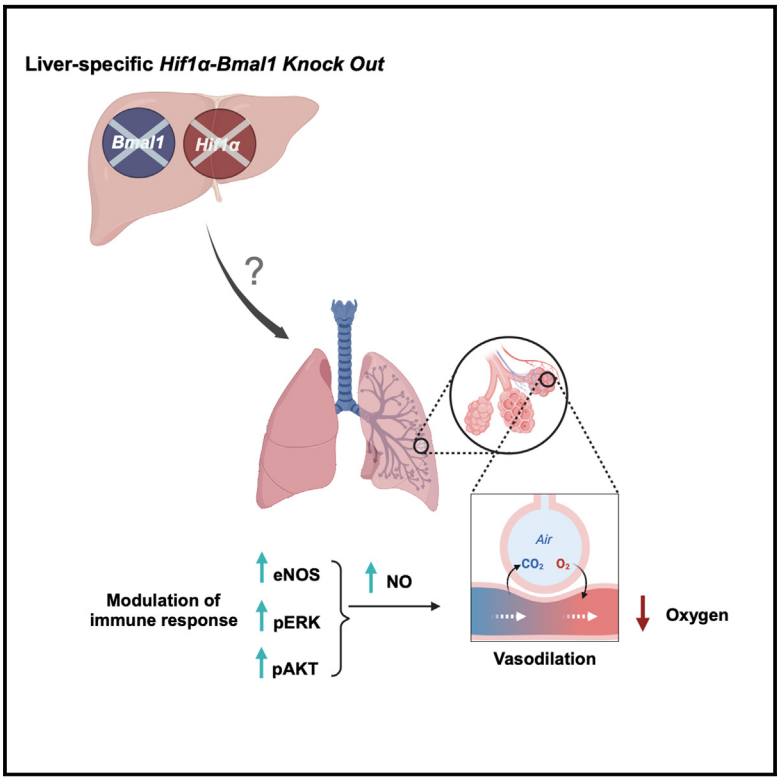

Authors

Vaishnavi Dandavate, Nityanand Bolshette, Rachel Van Drunen, ..., Marina Golik, Yaarit Adamovich, Gad Asher

Correspondence

gad.asher@weizmann.ac.il

In brief

Dandavate et al. found that the transcriptional response to hypoxia in the liver is largely dependent on *Bmal1* or *Hif1α*. Remarkably, mice lacking hepatic *Bmal1-Hif1α* are hypoxemic and exhibit increased daytime-dependent mortality upon hypoxic exposure. These mice exhibit characteristics of hepatopulmonary syndrome with increased pulmonary NO and vasodilation.

Highlights

- The liver transcriptional response to hypoxia is largely dependent on *Bmal1* or *Hif1α*
- Hepatic *Bmal1-Hif1α*-deficient mice exhibit daytime-dependent mortality upon hypoxia
- Hepatic *Bmal1-Hif1α*-deficient mice show characteristics of hepatopulmonary syndrome
- Hepatic *Bmal1-Hif1α*-deficient mice show increased pulmonary NO and vasodilation

Dandavate et al., 2024, Cell Metabolism *36*, 1–16
September 3, 2024
https://doi.org/10.1016/j.cmet.2024.07.003

CellPress

Cell Metabolism

CellPress

Article

Hepatic BMAL1 and HIF1α regulate a time-dependent hypoxic response and prevent hepatopulmonary-like syndrome

Vaishnavi Dandavate,[1,3] Nityanand Bolshette,[1,3] Rachel Van Drunen,[1] Gal Manella,[1] Hanna Bueno-Levy,[2] Mirie Zerbib,[2] Ippei Kawano,[1] Marina Golik,[1] Yaarit Adamovich,[1] and Gad Asher[1,4,*]

[1]Department of Biomolecular Sciences, Weizmann Institute of Science, 7610001 Rehovot, Israel
[2]Department of the Veterinary Resources, Weizmann Institute of Science, 7610001 Rehovot, Israel
[3]These authors contributed equally
[4]Lead contact
*Correspondence: gad.asher@weizmann.ac.il
https://doi.org/10.1016/j.cmet.2024.07.003

SUMMARY

The transcriptional response to hypoxia is temporally regulated, yet the molecular underpinnings and physiological implications are unknown. We examined the roles of hepatic *Bmal1* and *Hif1α* in the circadian response to hypoxia in mice. We found that the majority of the transcriptional response to hypoxia is dependent on either *Bmal1* or *Hif1α*, through shared and distinct roles that are daytime determined. We further show that hypoxia-inducible factor (HIF)1α accumulation upon hypoxia is temporally regulated and *Bmal1* dependent. Unexpectedly, mice lacking both hepatic *Bmal1* and *Hif1α* are hypoxemic and exhibit increased mortality upon hypoxic exposure in a daytime-dependent manner. These mice display mild liver dysfunction with pulmonary vasodilation likely due to extracellular signaling regulated kinase (ERK) activation, endothelial nitric oxide synthase, and nitric oxide accumulation in lungs, suggestive of hepatopulmonary syndrome. Our findings indicate that hepatic BMAL1 and HIF1α are key time-dependent regulators of the hypoxic response and can provide molecular insights into the pathophysiology of hepatopulmonary syndrome.

INTRODUCTION

Circadian clocks regulate various aspects of physiology and metabolism in mammals and enable them to adapt and synchronize with daily rhythmic environmental changes.[1–4] The molecular clockwork relies on a transcription-translation feedback loop with the transcription factors CLOCK and BMAL1 (brain and muscle Arnt-like 1) as positive regulators and PERIODs and CRYPTOCHROMESs as repressors, alongside an auxiliary feedback loop, which consists of REV-ERBs (NR1D1/2) and retinoic acid-related orphan receptors (RORs).[5–8] In recent years, growing evidence supports molecular and functional interactions between the circadian clock and oxygen signaling, in particular BMAL1 and HIF (hypoxia-inducible factor), respectively.[9–11] The clock regulates daily oscillation in oxygen consumption and tissue oxygenation predominantly through rest-activity and feeding-fasting cycles.[12] Concurrently, rhythmic oxygen levels serve as a time signal and synchronize clocks in a HIF1α-dependent manner.[13] Moreover, the transcriptional response to hypoxia and specifically the response of the molecular clock is tissue specific and daytime dependent.[14,15] Consequently, hypoxia, as in obstructive sleep apnea, elicits internal circadian misalignment.[14,16] At the molecular level, physical interaction between circadian clock components and oxygen signaling was first reported for BMAL1 and HIF1α.[17,18] Recently, additional clock proteins were shown to bind HIFs[17,19–21] and were implicated in the response to hypoxia mostly in cultured cells.[13,22,23]

Despite the growing evidence for interactions between the circadian clock and oxygen signaling, several aspects remain uncharted, in particular, the molecular and physiological implications *in vivo*.[9,10] To address these questions, we utilized liver-specific single and generated double knockout mice of *Bmal1* and *Hif1α* to examine their daytime-dependent response to hypoxia. We found that in the liver, the transcriptional response to hypoxia is largely dependent on *Bmal1* or *Hif1α*, through common and unique roles that are daytime dependent. Furthermore, *Bmal1* is necessary for the temporal accumulation of HIF1α upon hypoxia. Unexpectedly, hepatic *Bmal1-Hif1α*-deficient mice exhibit increased daytime-dependent mortality upon hypoxia and show physiological and molecular manifestations that are suggestive of hepatopulmonary syndrome (HPS).

Please cite this article in press as: Dandavate et al., Hepatic BMAL1 and HIF1α regulate a time-dependent hypoxic response and prevent hepatopulmonary-like syndrome, Cell Metabolism (2024), https://doi.org/10.1016/j.cmet.2024.07.003

RESULTS

The hypoxic response of clock and canonical HIF1α target genes is temporally regulated by BMAL1 and HIF1α

We previously reported that in the liver, several clock and canonical HIF1α target genes respond to hypoxia in a daytime-dependent manner.[14] Here, we examined whether the transcriptional response of these genes to hypoxia *in vivo* is regulated in a temporal manner by BMAL1, a key transcription factor within the clockwork,[24–27] or HIF1α, a principal regulator of the transcriptional response to hypoxia.[28] To this end, we employed liver-specific knockout mouse models of *Bmal1* (BLKO; *AlbCre*$^{+}$ *Bmal1*$^{fl/fl}$)[29,30] and *Hif1α* (HLKO; *AlbCre*$^{+}$ *Hif1α*$^{fl/fl}$),[31,32] alongside AlbCRE control mice. Mice were exposed to normoxia (21% oxygen) or hypoxia (6% oxygen) for 4 h, either in the subjective light (circadian time [CT] 4–8) or subjective dark phase (CT16–20) (Figure 1A).

Analysis of clock and canonical HIF1α target genes expression by qPCR (Figures 1B–1D and S1) in control mice showed, in line with our previous report,[14] that some genes respond to hypoxia in a daytime-dependent manner. *Per1* and *Cry2* showed a comparable response to hypoxia both at CT4–8 and CT16–20 (Figures 1B and S1B). Interestingly, this response was *Bmal1* and *Hif1α* dependent exclusively at CT16–20. Canonical HIF1α target genes (Figures 1C and S1C), such as *Egln3*, *Glut1*, and to a lesser extent, *Pdk1*, followed a similar trend as their response to hypoxia was reduced in the absence of *Bmal1* and *Hif1α* only at CT16–20. Thus, it appears that *Bmal1* and *Hif1α* control the response of these genes to hypoxia in a daytime-dependent manner. For clock genes that showed a daytime-dependent response to hypoxia, such as *Dbp* and *Chrono*, we found that both their basal expression and their response to hypoxia were mostly reduced in the livers of BLKO mice (Figures 1B and S1B). This is in line with the known role of BMAL1 in regulating their expression levels.[5,7] Last, the response of *Clock* and *Cry1* (Figure S1A and S1D) to hypoxia was independent of both *Bmal1* and *Hif1α*. As expected, the expression of *Bmal1* and *Hif1α* was diminished in the respective liver-specific knockout mice (Figures 1D and S1E).

Taken together, these results reveal an intricate time-dependent role of *Bmal1* and *Hif1α* in the transcriptional response to hypoxia. HIF1α controls the hypoxic response of clock and canonical HIF1α target genes mostly in the subjective dark phase, whereas BMAL1 is implicated both in basal expression and in response to hypoxia.

BMAL1 and HIF1α temporally regulate the global transcriptional response to hypoxia

In the liver, the overall transcriptional response to hypoxia is daytime dependent.[14] To dissect the general roles of BMAL1 and HIF1α in the temporal regulation of the hypoxic response, we performed genome-wide transcriptomic analysis (RNA sequencing [RNA-seq]) of livers from AlbCRE control, BLKO, and HLKO mice exposed to 4 h normoxia or hypoxia, either at CT4–8 or CT16–20 (Figure 1A). Principal component analysis (PCA) showed a clear segregation between the hypoxic and normoxic conditions and, to a lesser extent, between the different genotypes and time of day (Figure 2A). For subsequent analysis of differentially regulated genes, we used the following criteria: pair-wise analysis with adjusted $p < 0.05$ and $|\log \text{fold change}| > 1$. In normoxia, both BLKO and HLKO mice differed in their gene expression relative to control mice. These differences were more prevalent at CT4–8 compared with CT16–20 for both genotypes (Figure S2A) and were, to some extent, related to lipid metabolism (Figure S2B). Similar to control mice, hypoxia elicited daytime-dependent changes in gene expression in BLKO and HLKO mice (Figures S2C–S2E). BLKO mice exhibited an overall reduced response to hypoxia, with a higher response at CT16–20 compared with CT4–8 (Figures S2C and S2D). In HLKO mice, an opposite trend was observed with a lower response at CT16–20 compared with CT4–8 (Figures S2C and S2E). These findings hinted toward time-dependent roles of BMAL1 and HIF1α in the overall transcriptional response to hypoxia.

To further examine the genotype and daytime dependency of the transcriptional response to hypoxia, we clustered the hypoxic genes according to their expression profiles (Figure 2B). We identified the following cohorts: (1) genes that respond to hypoxia in knockouts similar to control, (2) genes that respond to hypoxia in control but lose their response in either BLKO or HLKO, and (3) genes that gain response to hypoxia in either BLKO or HLKO. Next, to dissect the dependency of the hypoxic response on *Bmal1* or *Hif1α*, we centered our analyses on genes that respond to hypoxia in control mice, i.e., groups I and II, and dissected the dependency of the hypoxic response on *Bmal1* or *Hif1α*. Both at CT4–8 and CT16–20, the bulk share of the transcriptional response to hypoxia was *Bmal1* or *Hif1α* dependent (i.e., 77% and 84%, respectively) (Figures 2C and 2D). *Bmal1* appears to be at par with *Hif1α* in regulating the hypoxic response (*Bmal1* dependency, 72% and 62% in subjective light and dark phases, respectively; *Hif1α* dependency, 52% and 71% in subjective light and dark phases, respectively). About 50% of the hypoxic genes in control mice lost their hypoxic response in both BLKO or HLKO mice, irrespective of time, suggesting a major shared role of BMAL1 and HIF1α in the transcriptional response to hypoxia (Figures 2C and 2D). The observed shared role of BMAL1 and HIF1α raises the possibility that they might act together or function upstream of each other upon hypoxia. Notably, at CT4–8, 25% of the hypoxic genes were exclusively dependent on *Bmal1* while only 5% were uniquely *Hif1α* dependent (Figure 2C), although at CT16–20, an opposite trend was detected with 22% of the hypoxic genes exclusively *Hif1α* dependent, and only 13% uniquely *Bmal1* dependent (Figure 2D). Hence, aside from their shared role in the transcriptional response to hypoxia, BMAL1 and HIF1α also carry distinct roles that are daytime dependent with dominance of BMAL1 and HIF1α at CT4–8 and CT16–20, respectively. The time-dependent roles of these two transcription factors were further detailed by a small overlap of dependent genes between the two time points (i.e., uniquely *Bmal1*, uniquely *Hif1α*, or both) (Figure S2F).

Enrichment analysis of transcripts that are commonly regulated by BMAL1 and HIF1α unveiled some pathways related to histone modifications and lipid metabolism (Figure 2E; Data S2D; up- and downregulated pathways are listed in Data S2E). Uniquely *Hif1α*-dependent transcripts were enriched for cytokine-mediated signaling (Figure 2F; Data S2D; up- and downregulated pathways are listed in Data S2E), whereas uniquely

Please cite this article in press as: Dandavate et al., Hepatic BMAL1 and HIF1α regulate a time-dependent hypoxic response and prevent hepatopulmonary-like syndrome, Cell Metabolism (2024), https://doi.org/10.1016/j.cmet.2024.07.003

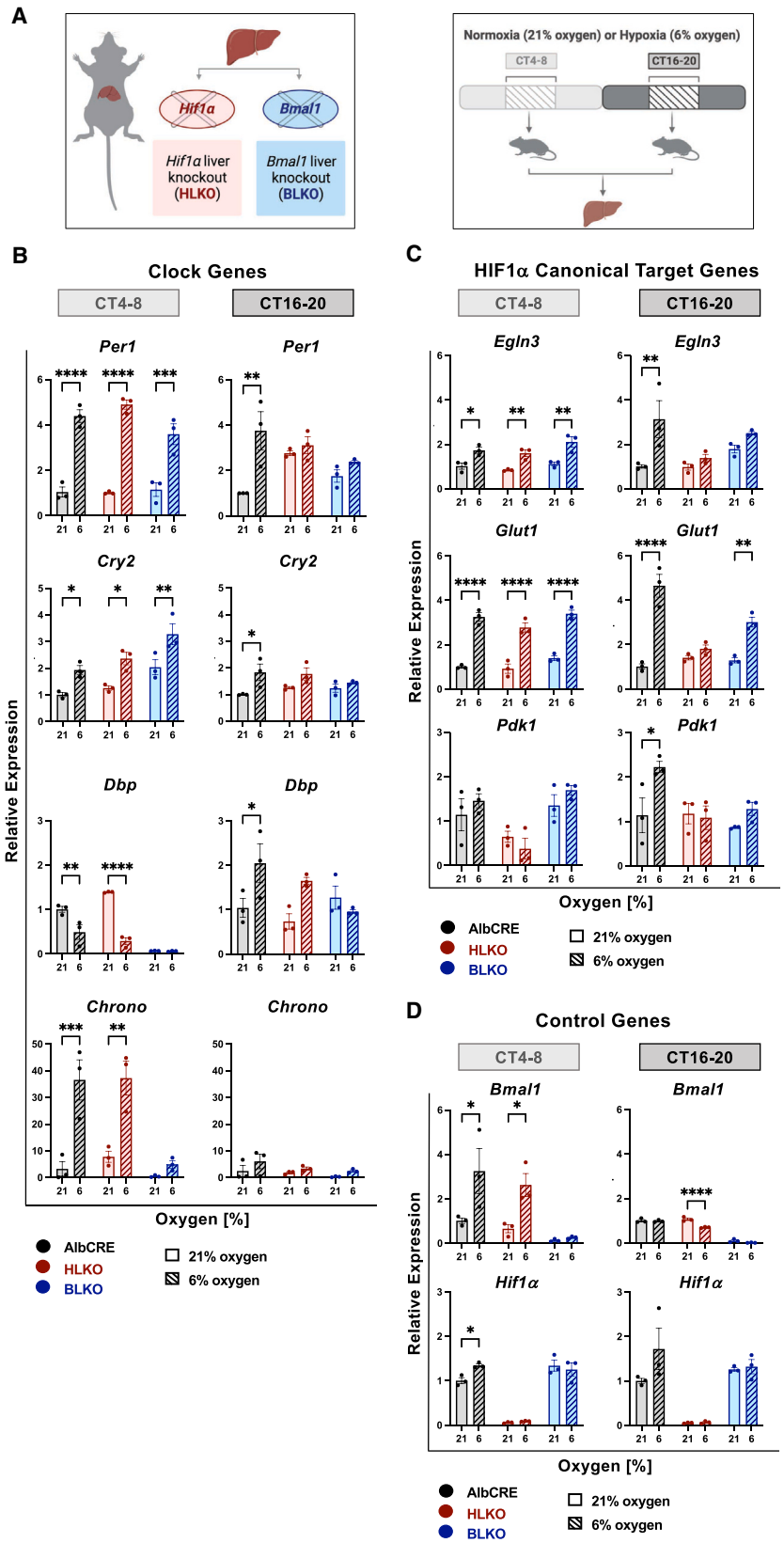

Figure 1. The hypoxic response of clock and canonical HIF1α target genes is temporally regulated by BMAL1 and HIF1α

(A) Schematic representation of the experimental design.

(B–D) Control mice (AlbCRE), liver-specific *Hif1α* knockout (HLKO), and liver-specific *Bmal1* knockout (BLKO) mice were exposed to 4 h of either normoxia (21% oxygen) or hypoxia (6% oxygen) in the subjective light (CT4–8) or subjective dark (CT16–20) phase. Animals were sacrificed, livers were harvested, and RNA was prepared and analyzed by qPCR for transcript levels of (B) Clock genes, (C) HIF1α canonical target genes, and (D) control genes.

Data are presented as the mean ± SEM, normalized to AlbCRE normoxia condition per time per gene; $n = 3$ per condition per genotype. Two-way ANOVA with Šídák's multiple comparisons post hoc test; $^{****}p < 0.0001$, $^{***}p < 0.001$, $^{**}p < 0.01$, $^{*}p < 0.05$. Graphical illustrations were generated with BioRender.com.

Please cite this article in press as: Dandavate et al., Hepatic BMAL1 and HIF1α regulate a time-dependent hypoxic response and prevent hepatopulmonary-like syndrome, Cell Metabolism (2024), https://doi.org/10.1016/j.cmet.2024.07.003

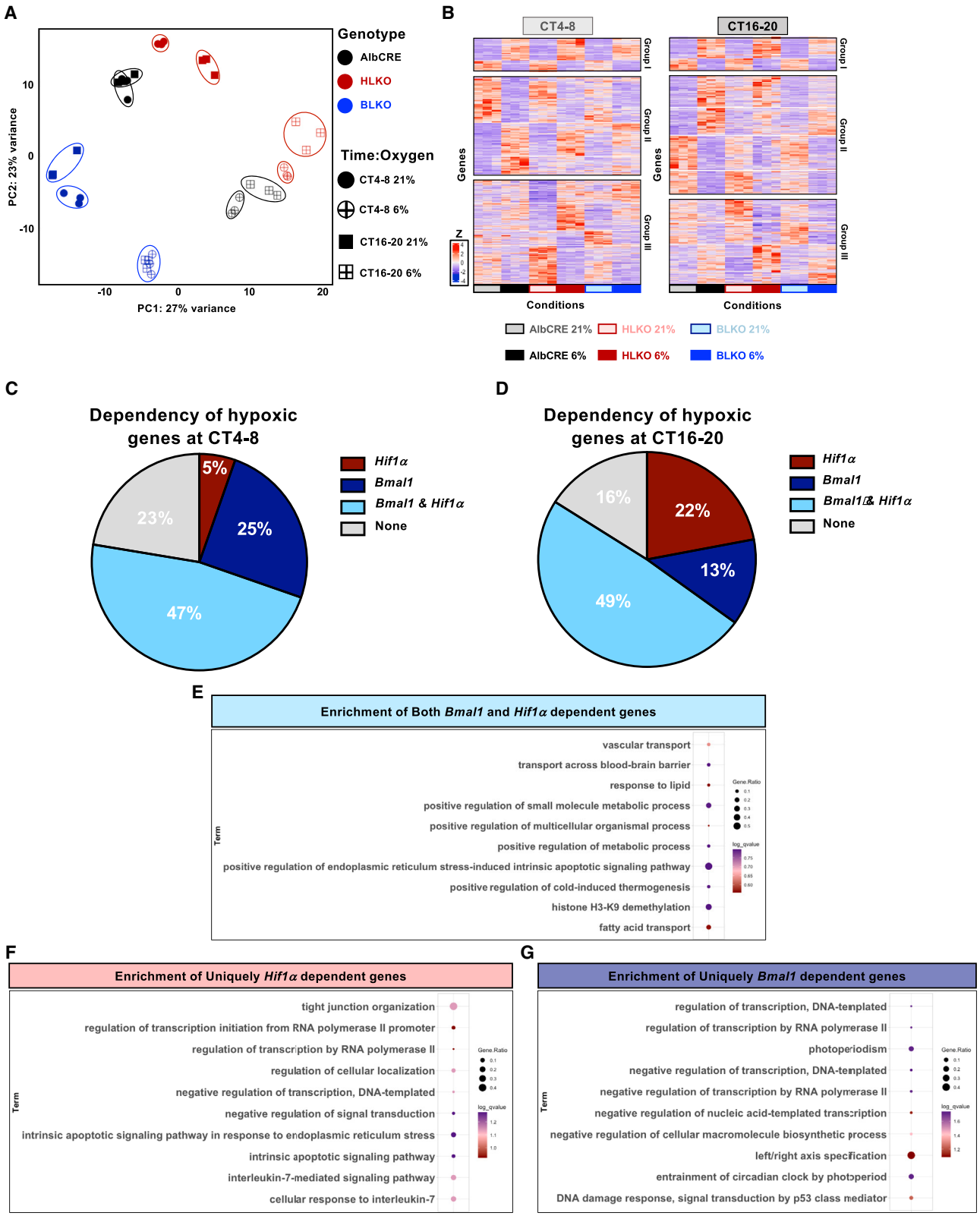

Figure 2. BMAL1 and HIF1α regulate the overall transcriptional response to hypoxia in a daytime-dependent manner

(A) PCA plot of the different mouse genotypes (AlbCRE, HLKO, and BLKO) under normoxia (21% oxygen) or hypoxia (6% oxygen) at CT4–8 or CT16–20, $n = 3$ mice per genotype per condition.

(legend continued on next page)

Please cite this article in press as: Dandavate et al., Hepatic BMAL1 and HIF1α regulate a time-dependent hypoxic response and prevent hepatopulmonary-like syndrome, Cell Metabolism (2024), https://doi.org/10.1016/j.cmet.2024.07.003

Bmal1-dependent genes showed circadian- and RNA polymerase-related pathways (Figure 2G; Data S2D; up- and downregulated pathways are listed in Data S2E).

Overall, our analyses indicate that BMAL1 and HIF1α play a principal role in the global transcriptional response to hypoxia whereby a major part of the response is shared by both BMAL1 and HIF1α. A subset of genes is exclusively controlled by either BMAL1 or HIF1α in a daytime-dependent manner. The former plays a more prominent role in the subjective light phase, whereas the latter is more dominant in the subjective dark phase.

Accumulation of liver HIF1α upon hypoxia is time and Bmal1 dependent

Both BMAL1 and HIF1α are members of the basic helix-loop-helix (bHLH) and Per-Arnt-Sim (bHLH-PAS) domain-containing transcription factors.[9,11,17,33] BMAL1 and HIF1α were previously reported to physically interact with each other,[18,22] and recently, BMAL1 was shown to support the accumulation of HIF1α upon exposure of myotubes to hypoxia in cell culture.[23] This, along with our findings that the transcriptional response to hypoxia in mouse liver is highly dependent on *Bmal1* and *Hif1α* in a daytime-dependent manner, prompted us to examine their protein levels *in vivo* in response to hypoxia. We first examined the nuclear accumulation of BMAL1 and HIF1α in the liver of control mice upon exposure to 4 h hypoxia either at CT4–8 or CT16–20. HIF1α accumulation upon hypoxia was daytime dependent, with higher accumulation at CT16–20 compared with CT4–8 (Figure 3A). As the transcript levels of *Hif1α* upon hypoxia only slightly differed at CT16–20 compared with CT4–8 (Figure S1E), it is likely that the effect is mediated post-transcriptionally. At both time points, BMAL1 nuclear-protein levels were altered upon hypoxia; in particular, the hyper-phosphorylated form appeared to accumulate (Figure 3A).

To elucidate the potential inter-dependency between BMAL1 and HIF1α upon hypoxia, we took advantage of our genetic mouse models and examined the dependency of HIF1α accumulation on *Bmal1* as well as BMAL1 hyper-phosphorylation on *Hif1α*. To this end, we tested nuclear-protein extracts of control, HLKO, and BLKO mice, exposed to hypoxia either at CT4–8 or CT16–20. In the absence of *Bmal1*, HIF1α accumulation was abolished regardless of the time (Figures 3B and 3C). As *Hif1α* transcript levels were unaffected in BLKO mice compared with control mice (Figure 1D), it is conceivable that BMAL1 supports HIF1α stability. Notably, we cannot exclude the possibility that there is still some residual accumulation of HIF1α in the absence of *Bmal1*, which is not detected due to low antibody detection capacity and would explain the transcriptional response to hypoxia that is exclusively HIF1α dependent.

We next tested if *Hif1α* plays a role in BMAL1 phosphorylation under hypoxia. Contrary to HIF1α, the pattern observed for BMAL1 was similar in HLKO mice, and the hyperphosphorylated form accumulated both in total and nuclear liver extracts upon hypoxia irrespective of time (Figures 3B, 3C, and S3A). BMAL1 as expected was not detected in BLKO mice, and HIF1α was not spotted in total liver extracts, likely due to its low abundance (Figures 3B, 3C, and S3B).

We concluded that HIF1α accumulation upon hypoxia in mouse liver is temporally regulated and *Bmal1* dependent, whereas BMAL1 phosphorylation under hypoxia is *Hif1α* independent. As up to 50% of the transcriptional response to hypoxia depends on both *Bmal1* and *Hif1α*, it is likely that their functional interaction stems from the dependency of HIF1α accumulation upon hypoxia on *Bmal1*.

Mice deficient in hepatic Bmal1 and Hif1α show a daytime-dependent mortality in response to hypoxia

Our findings that *Bmal1* and *Hif1α* control the majority of the transcriptional response to hypoxia in the liver led us to examine their mutual effect on the hypoxic response. To this end, we generated the liver-specific knockout mouse model for both *Bmal1* and *Hif1α* (BHLKO; *AlbCre*$^{+}$ *Bmal1*$^{fl/fl}$ *Hif1α*$^{fl/fl}$) (Figure S4A). BHLKO and HLKO weighed more compared with age-matched AlbCRE and BLKO mice (Figure S4B). Body composition analysis did not identify any significant changes in their relative fat mass, lean mass, or free fluid (Figure S4B).

Animals were exposed to hypoxia, as described above (Figure 1A), either at CT4–8 or CT16–20. Unexpectedly, at CT16, none of the BHLKO mice survived 4 h of hypoxia (Figure 4A). Within the first 30 min of hypoxic exposure at CT16, BHLKO mice exhibited 50% mortality, whereas no mortality was observed at CT4 within this time window (Figure 4B). Some mortality was also seen with HLKO mice but to a much lesser extent, and no mortality with control or BLKO mice. We concluded that the absence of hepatic *Bmal1* and *Hif1α* reduces the ability of mice to cope with hypoxic exposure in a daytime-dependent manner.

To identify the potential cause for the increased mortality of BHLKO mice in response to hypoxia, we centered our attention first on the liver, where *Bmal1* and *Hif1α* were knocked out (Figure S4A). As mortality was observed within the first 30 min of hypoxic exposure at CT16, we postulated that these mice suffer from a pathological predisposition that might be detected already upon normoxia at CT16. We did not detect any overt histological differences in livers of any of the knockout mice compared with control mice (Figure S4C). Next, we performed a series of tests to evaluate liver functions at both CT4 and CT16 under normoxia (Figures 4C, 4D, S4D, and S4E).[34] The levels of liver enzymes SGOT, SGPT, alkaline phosphatase, lactate dehydrogenase, and liver triglycerides were unaffected in any of the knockouts (Figures S4D and S4E). We did identify some significant changes in total bilirubin, total protein, albumin, and globulin levels particularly in BHLKO mice; however, these changes were within the normal physiological range, except for

(B) Heatmaps represent genes that significantly changed, clustered by their expression pattern (pair-wise analysis, adjusted $p < 0.05$ and |log fold change| > 1), upon hypoxia in either one of the genotypes (see the list of differentially regulated genes in Data S2A and cluster genes in Data S2B).
(C and D) Pie chart representation of genes that responded to hypoxia in AlbCRE and lose their hypoxic response in HLKO, BLKO, or both, termed as *Bmal1*-, *Hif1α*-, and *Bmal1*- and *Hif1α*-dependent genes, respectively, at (C) CT4–8 and (D) CT16–20 (see gene lists in Data S2C).
(E–G) Enrichment analysis of genes by EnrichR (see pathway list in Data S2D and S2E), which are (E) both *Bmal1* and *Hif1α* dependent, (F) uniquely *Hif1α* dependent, or (G) uniquely *Bmal1* dependent irrespective of the daytime.

Please cite this article in press as: Dandavate et al., Hepatic BMAL1 and HIF1α regulate a time-dependent hypoxic response and prevent hepatopulmonary-like syndrome, Cell Metabolism (2024), https://doi.org/10.1016/j.cmet.2024.07.003

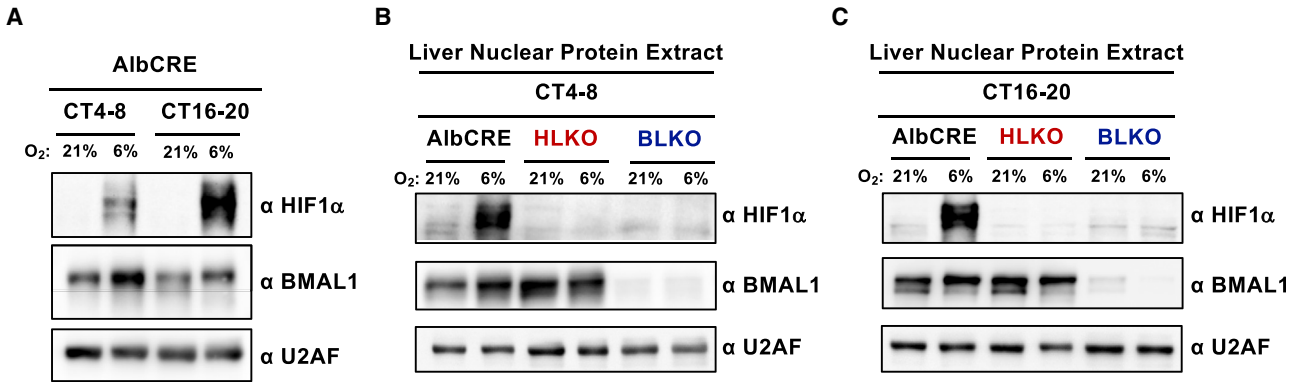

Figure 3. HIF1α accumulation upon hypoxia is time and *Bmal1* dependent

(A) Immunoblot analyses of BMAL1 and HIF1α in liver nuclear extracts from control mice (AlbCRE) exposed to either normoxia (21% oxygen) or hypoxia (6% oxygen) for 4 h at CT4–8 or CT16–20.

(B and C) Immunoblot analyses of BMAL1 and HIF1α in liver nuclear extracts from control mice (AlbCRE), liver-specific *Hif1α* knockout (HLKO), and liver-specific *Bmal1* knockout (BLKO) mice exposed to either normoxia (21% oxygen) or hypoxia (6% oxygen) for 4 h at (B) CT4–8 and (C) CT16–20. A pool of $n = 3$ animals was used per condition per genotype. The AlbCRE samples in (B) and (C) are the same from (A).

albumin in BHLKO mice at CT16[35,36] (Figures 4C and 4D). BHLKO mice also showed some mild differences, yet within the physiological range, in key blood electrolytes, such as potassium, chlorine, and phosphorous relative to control mice, mostly at CT16 (Figures 4E and 4F). These changes were unlikely due to kidney malfunction, as urea and creatinine levels were normal (Figures S4F and S4G).[37] No significant changes in blood cholesterol and triglyceride levels were detected (Figures S4H and S4I), and blood glucose levels were elevated in BHLKO exclusively at CT16 (Figures S4J and S4K).

Altogether, we found that mice lacking both hepatic *Bmal1* and *Hif1α* exhibit increased mortality upon exposure to hypoxia at CT16 compared with CT4. However, they show only a very mild liver dysfunction with hypoalbuminemia and some minor electrolyte misbalances mostly at CT16.

Mice deficient in hepatic Bmal1 and Hif1α exhibit characteristics of HPS

The increased mortality upon hypoxic exposure in liver-deficient *Bmal1* and *Hif1α* mice hinted at impaired oxygen metabolism. The vital role of the lungs in oxygen uptake through respiration raised the possibility that BHLKO mice have HPS. HPS is characterized by a triad of liver dysfunction, arterial hypoxemia, and intrapulmonary vasodilation.[38,39] The syndrome is prevalent among humans with different degrees of liver disease. We first histologically characterized the lungs and did not reveal any overt differences in BHLKO or single liver-knockout models (Figure S5A). Mixed blood gas analysis revealed that blood oxygen saturation levels are severely dampened (Figure 5A). Partial CO_2 pressure was elevated in BHLKO mice compared with control and single knockout mice; however, it remained within the normal physiological range (Figure 5A).[40] Bicarbonate levels were slightly elevated likely as a compensatory mechanism to maintain normal pH (Figure 5A). No significant differences in blood hemoglobin concentration or hematocrit were observed (Figure S5B). We concluded that mice lacking both hepatic *Bmal1* and *Hif1α* are severely hypoxemic and already in normoxia.

Next, we examined whether these mice exhibit intrapulmonary vasodilation. The gold standard methodology for the detection of pulmonary vasodilation in humans is echocardiography alongside peripheral vein microbubbles injection.[41–43] Usually, microbubbles are trapped in the pulmonary circulation and absorbed by the alveoli. However, in the presence of pulmonary vasodilation, microbubbles evade pulmonary capture and reach the heart faster as can be detected by echocardiography (Figure 5B). We set out to establish a similar assay in mice and monitored the appearance of injected microbubbles in the left ventricle by echocardiography. We found that microbubbles reach the heart faster in BHLKO compared with control mice (Figure 5C; Video S1), supporting the presence of pulmonary vasodilation in these mice. Although our echocardiography identified an increase in left ventricle volume in BHLKO mice, we did not detect overt functional consequences as both systolic and diastolic functions remained similar (Figure S5C; Table S1). Notably, the ratio between the pulmonary (Qp) and the systemic (Qs) blood flow did not significantly differ between AlbCRE control and BHLKO mice, excluding an intracardiac shunt and favoring intrapulmonary vasodilatation.[44,45]

We concluded that mice lacking both hepatic *Bmal1* and *Hif1α* exhibit characteristics consistent with HPS as they show some mild liver dysfunction, are hypoxemic, and exhibit intrapulmonary vasodilation.

ERK activation, eNOS, and NO accumulation in the lungs of mice deficient in hepatic Bmal1 and Hif1α

Our findings that mice lacking both hepatic *Bmal1* and *Hif1α* exhibit hallmarks of HPS prompted us to further characterize the molecular changes in the lungs of these mice. We first tested the expression of *Bmal1* and *Hif1α* in the BHLKO lungs and did not see any significant differences (Figure S6A).

HPS has been associated with accumulation of endothelial nitric oxide synthase (eNOS), a key enzyme in production of nitric oxide (NO),[46] which elicits intrapulmonary vasodilation.[47,48] We examined the lung protein levels of eNOS in normoxia and found that they are elevated in BHLKO mice at CT16 (Figure 6A) and, to

Please cite this article in press as: Dandavate et al., Hepatic BMAL1 and HIF1α regulate a time-dependent hypoxic response and prevent hepatopulmonary-like syndrome, Cell Metabolism (2024), https://doi.org/10.1016/j.cmet.2024.07.003

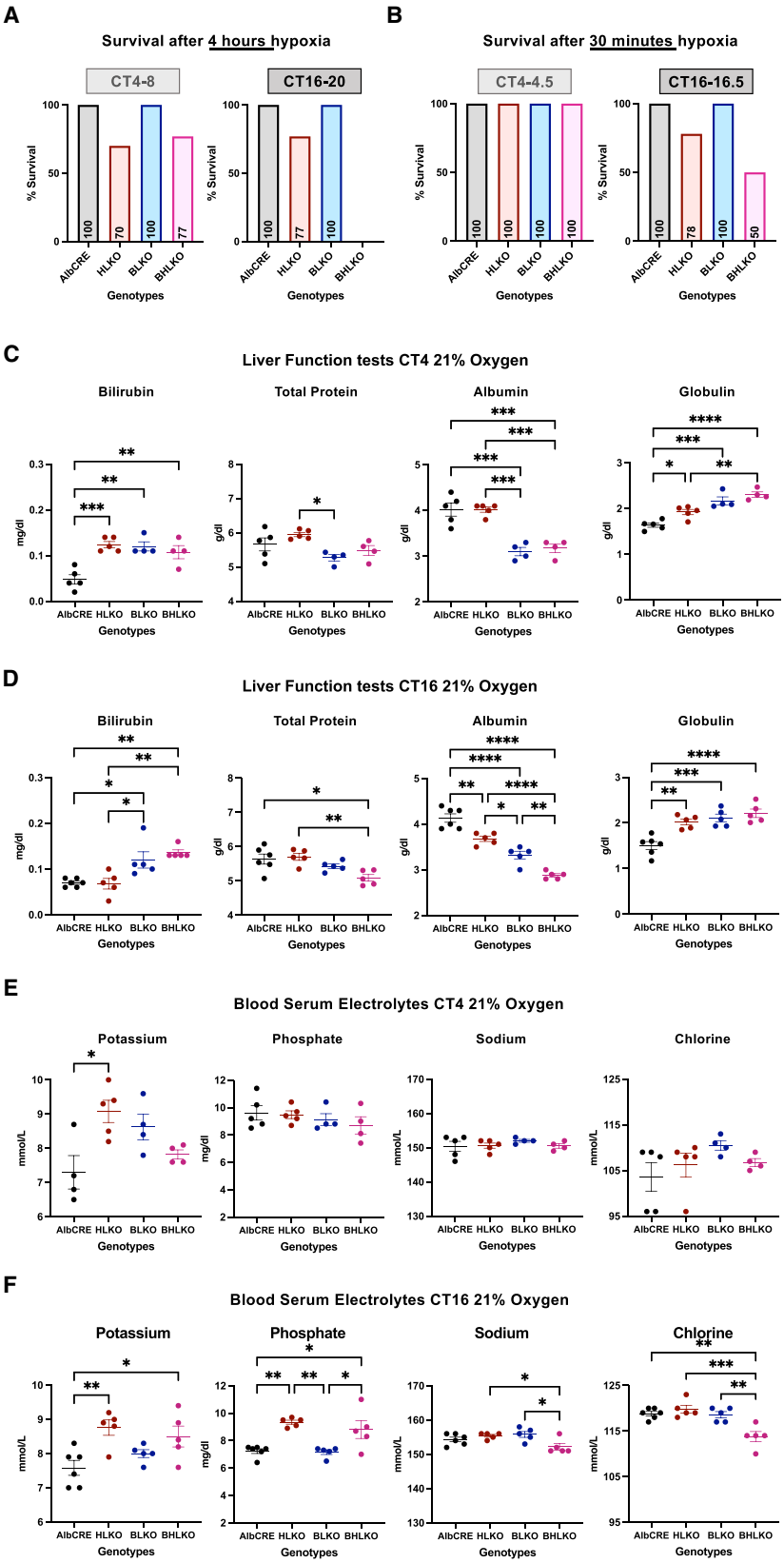

Figure 4. Liver-specific *Bmal1* and *Hif1α* knockout mice exhibit daytime-dependent mortality in response to hypoxia

(A and B) Bar plots representing the survival rates of control mice (AlbCRE), liver-specific *Hif1α* knockout (HLKO), liver-specific *Bmal1* knockout (BLKO), or liver-specific *Bmal1* and *Hif1α* knockout (BHLKO) mice in response to (A) 4 h ($p < 0.001$) and (B) 30 min ($p < 0.001$) hypoxia (6% oxygen) at CT4 or CT16 (n = 10–15 mice per genotype per CT); chi-squared test.

(C and D) Blood serum liver-function tests of AlbCRE, HLKO, BLKO, and BHLKO mice under normoxia at (C) CT4 and (D) CT16.

(E and F) Blood serum electrolyte measurements of AlbCRE, HLKO, BLKO, and BHLKO mice under normoxia at (E) CT4 and (F) CT16.

In (C)–(F), data are presented as the mean ± SEM, n = 5–6 mice per genotype; one-way ANOVA with Tukey's post hoc test, $^{****}p < 0.0001$, $^{***}p < 0.001$, $^{**}p < 0.01$, $^{*}p < 0.05$.

Please cite this article in press as: Dandavate et al., Hepatic BMAL1 and HIF1α regulate a time-dependent hypoxic response and prevent hepatopulmonary-like syndrome, Cell Metabolism (2024), https://doi.org/10.1016/j.cmet.2024.07.003

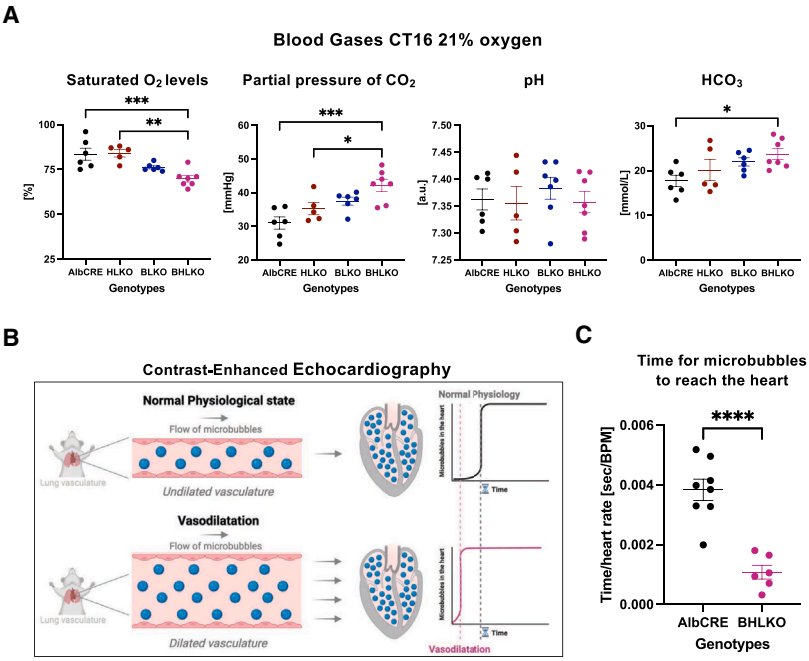

Figure 5. Liver-specific *Bmal1* and *Hif1α* knockout mice exhibit characteristics of hepatopulmonary syndrome

(A) Mixed blood oxygen saturation, carbon dioxide partial pressure, pH, and bicarbonate (HCO_3) levels measured in control mice (AlbCRE), liver-specific *Hif1α* knockout (HLKO), liver-specific *Bmal1* knockout (BLKO), or liver-specific *Bmal1* and *Hif1α* knockout (BHLKO) mice. Blood measurements were performed under normoxia at CT16 (mean ± SEM, n = 5–7 mice per genotype); one-way ANOVA with Tukey's post hoc test, $^{***}p < 0.001$, $^{**}p < 0.01$, $^{*}p < 0.05$.

(B) Graphical representation of a contrast-enhanced agent flow in normal vs. vasodilated pulmonary vasculature alongside a representation the time taken for the contrast agent (microbubbles) to reach the heart's left ventricle.

(C) Echocardiography measurements of the time taken for the microbubbles to reach the heart's left ventricle after injection, normalized by heart rate in AlbCRE vs. BHLKO mice around CT16 (mean ± SEM, n = 6–8 mice per genotype); Student's t test, $^{****}p < 0.0001$. Graphical illustration was generated with BioRender.com.

a lesser extent, at CT4 compared with other mouse strains (Figure S6B). Importantly, NO levels corresponded to eNOS levels and were specifically elevated in BHLKO mice at CT16 and not at CT4 (Figures 6B and S6C). Notably, inducible NOS (iNOS) was not affected in any of our mouse strains (Figure 6C). In rats with common bile duct ligation (CBDL)-induced HPS, elevated serum endothelin-1 (ET1) levels were suggested to stimulate eNOS.[49] Consistently, analysis of ET1 serum levels in the different mouse models, at CT16 under normoxia, identified elevated levels of ET1 in HLKO and BHLKO mice (Figure 6D).

Extracellular signaling regulated kinase (ERK) and protein kinase B (AKT) pathways have been proposed to play a role in pulmonary vasodilation in rats with CBDL-induced HPS.[38,50–52] We found that ERK phosphorylation at amino acid Thr202/Tyr204 is elevated in the lungs of our liver knockout mouse models, especially in BHLKO mice (Figure 6A). Basal AKT phosphorylation at amino acid Ser473 was slightly elevated both in HLKO and BHLKO mice and not in BLKO mice (Figure 6A). It is noteworthy that no effects on ERK and AKT basal phosphorylation levels were detected in liver or kidney samples of the different liver knockout mouse models from the same animals (Figures 6E and 6F), suggesting that these effects are lung specific and are not due to broad systemic effects. Similar to CBDL-induced HPS,[53] we observed a slight increase in the levels of proliferating cell nuclear antigen (PCNA) in the lungs of BHLKO mice (Figure S6D). Furthermore, analysis of serum circulating cytokine/chemokine revealed several changes, in particular elevated levels of several chemokines in BHLKO mice (e.g., CCL2, CCL5, and CXCL1) (Figure S6E), supporting modulation of the inflammatory response, in line with previous reports on HPS.[39]

To gain further insight into the molecular changes that occur in the lungs of the BHLKO mice, we performed genome-wide transcriptomic analysis. Gene expression analysis of AlbCRE and BHLKO lungs under normoxia at CT16 (Figure 6G) showed 204 genes differentially expressed in BHLKO mice, with 72 and 132 up- and downregulated, respectively (Figure 6H; Data S4A). Enrichment analysis of the differentially regulated genes in the lungs of BHLKO mice identified many immune-related pathways (Figure 6I; Data S4B).

BHLKO mice are hypoxemic under normoxia (Figure 5A). Comparison of differentially expressed genes (DEGs) in the BHLKO lungs with genes altered by 4 h hypoxic exposure in the lungs of wild-type mice[14] showed a small overlap between the two datasets (31 genes of 204 genes) (Figure S6F; Data S5). This hinted that the observed changes in the lungs are not a mere consequence of the hypoxemia in these mice. Likewise, exposure of AlbCRE control mice to hypoxia at CT16 induced a slight elevation in pulmonary eNOS and pERK levels; however, these effects were much milder compared with the one observed in BHLKO mice under normoxia (Figure S6G).

Taken together, our findings suggest that mice lacking hepatic *Bmal1* and *Hif1α* exhibit significant molecular changes in their lungs. These include ERK activation, eNOS, and NO accumulation as well as modulation of various immune-related pathways that are likely to play a role in the pathophysiology of HPS.

Lung single-cell RNA analysis of hepatic Bmal1- and Hif1a-deficient mice reveals changes in lung cell composition and gene expression

As detailed above, our whole-lung analysis in mice lacking both hepatic *Bmal1* and *Hif1α* revealed changes in various signaling pathways as well as immune-related gene expression. The heterogeneous nature of the lung consisting of various cell types, such as epithelial, mesenchymal, and a wide variety of immune cell types,[54,55] prompted us to perform single-cell RNA sequence analysis of the lungs of BHLKO mice and AlbCRE control mice. Three biological replicates were used per genotype (total of 6 lungs); after filtering, 22,741 cells were integrated and

Please cite this article in press as: Dandavate et al., Hepatic BMAL1 and HIF1α regulate a time-dependent hypoxic response and prevent hepatopulmonary-like syndrome, Cell Metabolism (2024), https://doi.org/10.1016/j.cmet.2024.07.003

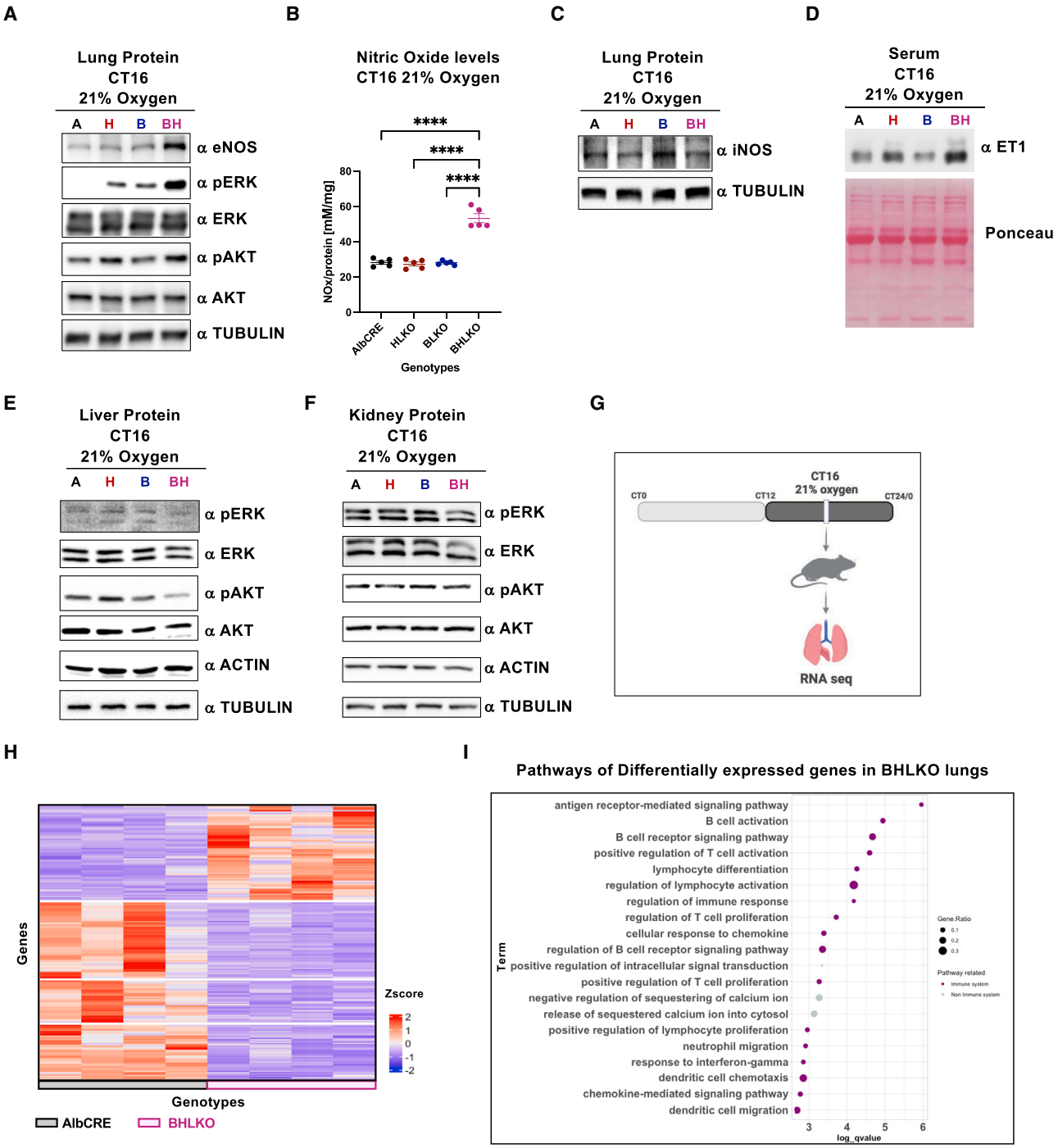

Figure 6. Molecular characterization of lungs of liver-specific *Bmal1* and *Hif1α* knockout mice

(A) Immunoblot analyses of total lung protein extracts from control mice (AlbCRE), liver-specific *Hif1α* knockout (HLKO), liver-specific *Bmal1* knockout (BLKO), or liver-specific *Bmal1* and *Hif1α* knockout (BHLKO) mice under normoxia at CT16 (pool of $n = 5$ mice per genotype).

(B) Nitric oxide (NO) measurements in lung tissues of AlbCRE, HLKO, BLKO, and BHLKO mice under normoxia at CT16 (mean ± SEM, $n = 5$ mice per genotype); one-way ANOVA with Tukey's post hoc test, $^{****}p < 0.0001$.

(C) Immunoblot analyses of iNOS in lung tissues of AlbCRE, HLKO, BLKO, and BHLKO mice under normoxia at CT16 (pool of $n = 5$ mice per genotype).

(D–F) (D) Immunoblot analysis of endothelin-1 (ET-1) in the serums of AlbCRE, HLKO, BLKO, and BHLKO mice under normoxia at CT16 (pool of $n = 5$ mice per genotype). Immunoblots of total (E) liver and (F) kidney protein extracts from AlbCRE, HLKO, BLKO, and BHLKO under normoxia at CT16 (pool of $n = 5$ mice per genotype).

(legend continued on next page)

Please cite this article in press as: Dandavate et al., Hepatic BMAL1 and HIF1α regulate a time-dependent hypoxic response and prevent hepatopulmonary-like syndrome, Cell Metabolism (2024), https://doi.org/10.1016/j.cmet.2024.07.003

analyzed (quality control steps are detailed in STAR Methods and depicted in Figures S7A–S7C; Data S6).

We identified 30 distinct clusters in both AlbCRE and BHLKO lungs, which were grouped into 12 distinct major cell types based on representative marker genes (Figures 7A and S7D; Table S2; Data S6). Cluster identities were largely consistent with previously reported single-cell lung datasets,[54,55] and cellular heterogeneity was preserved across genotypes and biological replicates (Figures S7B and S7C). The three largest cell populations, namely, endothelial, stromal, and epithelial cells, did not show apparent difference in their relative abundance between BHLKO and AlbCRE control lungs (Figure S7C). However, monocytes and erythroid precursor cells were less abundant in BHLKO lungs relative to AlbCRE control mice (Figure 7B). Moreover, we noted a trend wherein the relative abundance of the T cell population was higher in the BHLKO lungs compared with the AlbCRE lungs, whereas the B cell population showed an opposite trajectory (Figure 7B). Consequently, in the BHLKO lungs, the ratio of T to B cells nearly doubled that observed in the AlbCRE lungs. Thus, our finding that the abundance of the more pervasive endothelial and stromal cells in the lung is relatively similar between the two genotypes, excludes major structural changes. The changes in the abundance of some specific immune cell type populations alongside the observed changes in serum circulating cytokine/chemokine (Figure S6E) support the potential involvement of the immune system in the observed phenotype.

The lung single-cell RNA sequence analysis enabled us to dissect changes not only in cell abundance but also in their related gene expression. To this end, DESeq was carried out on the pseudobulked major cell clusters. Remarkably, although the abundance of endothelial cells, stromal cells, and alveolar macrophage did not vary between BHLKO and AlbCRE control lungs, these cell types exhibited the highest numbers of DEGs (Figure 7C). This suggests that the absence of *Bmal1* and *Hif1α* in liver elicits changes in gene expression within certain lung cell populations (Data S7 and S8). Although the numbers of upregulated and downregulated DEGs were nearly equal within endothelial cells and alveolar macrophages, stromal cells had close to twice as many downregulated DEGs compared with their upregulated DEGs (Figures 7D–7F). Functional enrichment analysis of the endothelial DEGs identified Gene Ontology (GO) pathways such as platelet activation, which are known to modulate the immune response[56,57] (Figure 7G). Another identified pathway is the regulation of viral entry that is comprised mostly of *Trim* genes, which are implicated in innate immunity[58] (Figures 7D and 7G). Both pathways are mainly characterized by downregulated DEGs in the BHLKO lungs (Figure S7F), supporting the suppression of immune-related pathways within these cells. In stromal cells, gene expression changes were related to leukocyte migration (Figures 7H and S7G). We also identified changes in mitogen-activated protein kinase (MAPK) cascade-related genes that may relate to the observed changes in ERK activation in the lungs of BHLKO mice (Figure 6A). In both stromal cells and alveolar macrophages, chemokines such as *Cxcl10*, *Cxcl14*, and *Cxcl1* were among the DEGs further supporting immune-related changes (Figures 7E, 7F, and S7G; Data S8). Interestingly, alveolar macrophages showed upregulation of DEGs such as *Gucy1a2*, *Gucy1b1*, and *Gucy1a1*, which are associated with cGMP and NO signaling pathways (Figures 7I and S7H), coinciding with our finding that lung eNOS and NO levels are elevated in BHLKO mice.

Taken together, these findings show that loss of *Bmal1* and *Hif1α* elicits changes in the lung cell population and cell-type-specific gene expression. These changes might play a role in the pathophysiology of HPS.

Expression of Serpina genes is altered in the livers of mice deficient in hepatic Bmal1 and Hif1α

It has been previously proposed that altered liver-lung communication is implicated in the pathophysiology of HPS likely through changes in secreted factors such as ET1 (Figure 6D).[38,39] As BHLKO mice exhibit characteristics of HPS and lack two key hepatic transcription factors, namely HIF1α and BMAL1, we hypothesized that analyzing changes in their hepatic gene expression, with special emphasis on secreted factors, might provide insight regarding potential mechanisms through which the liver communicates and modulates the function of the lungs. To this end, we performed genome-wide transcriptomic analysis (RNA-seq) of livers from BHLKO mice, normoxia at CT20, and compared them with AlbCRE, BLKO, and HLKO liver transcriptome (presented in Figures 2 and S2).

PCA showed a clear segregation between the genotypes (Figure S8A). BHLKO mice exhibited the highest number of DEGs, followed by BLKO and then HLKO mice (Figure S8B) with some overlap between the different genotypes (Figure S8C).

It is plausible that the liver communicates with the lung through a secreted protein; therefore, we narrowed our analysis to changes in the expression of genes that encode secretory proteins based on the GO database. BHLKO mice showed the highest number of DEGs within this category followed by BLKO and then HLKO mice (Figure S8D). We further focused on these genes that were common between HLKO and BHLKO mice as we observed hypoxia-induced mortality only in these two genotypes (Figures 5A and 5B). This resulted in eight genes (Figure S8E), out of which five belong to the SERPIN (serine protease inhibitors) family (*Serpina3c*, *Serpina3m*, *Serpina11*, *Serpina1d*, and *Serpina1e*) (Figure S8F). It is noteworthy that the human SERPINA1 gene encodes for α1-antitrypin, which is mainly produced in the liver, and its deficiency in a human genetic disorder results in pulmonary disease.[59,60]

Expression analysis of these five *Serpins* by quantitative PCR confirmed that *Serpina3c* and *Serpina11* are upregulated,

(G) Schematic depiction of experimental design, mice were sacrificed under normoxia at CT16, the lungs were harvested, and RNA was prepared and sequenced.

(H) Heatmap representation of differentially expressed genes in BHLKO compared with AlbCRE mice; threshold of adjusted $p < 0.05$ and $|\log_2 \text{foldchange}| > 1$ (see gene lists in Data S4A).

(I) Enrichment analysis of differentially expressed genes in BHLKO by EnrichR (see pathway list in Data S4B). Graphical illustration was generated with BioRender.com.

Please cite this article in press as: Dandavate et al., Hepatic BMAL1 and HIF1α regulate a time-dependent hypoxic response and prevent hepatopulmonary-like syndrome, Cell Metabolism (2024), https://doi.org/10.1016/j.cmet.2024.07.003

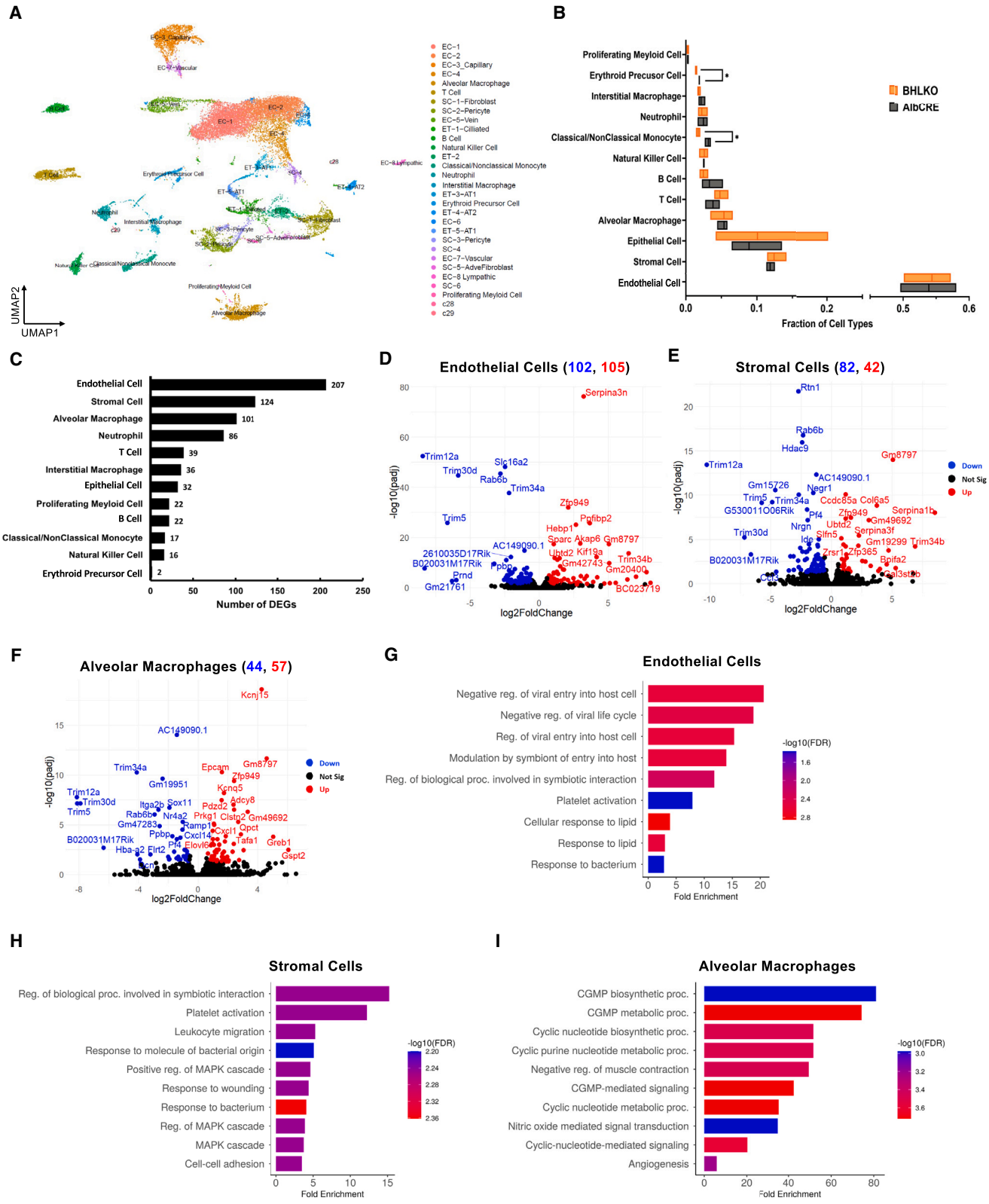

Figure 7. Lungs of liver-specific *Bmal1* and *Hif1a* knockout mice exhibit cell-specific changes in abundance and pathway enrichment

(A) UMAP of 22,741 cells from AlbCRE and BHLKO lungs harvested at CT16. Clusters are color labeled by cell type and number. Endothelial cells, ECs; stromal cells, SCs; epithelial cells, ETs.

(legend continued on next page)

Please cite this article in press as: Dandavate et al., Hepatic BMAL1 and HIF1α regulate a time-dependent hypoxic response and prevent hepatopulmonary-like syndrome, Cell Metabolism (2024), https://doi.org/10.1016/j.cmet.2024.07.003

whereas *Serpina3m* and *Serpina1e* are downregulated in HLKO and BHLKO mice (Figure S8G).

Thus, these results raise the possibility that the *Serpina* family genes could potentially be involved in the liver-lung communication and that alterations in their liver expression might affect the lungs and play a role in the pathophysiology of HPS.

DISCUSSION

Oxygen biology and circadian rhythms, with HIF1α and BMAL1, respectively, have been increasingly linked in recent years.[9,11] However, the molecular and physiological relevance of their interaction *in vivo* is largely unknown. In this study, we show that BMAL1 and HIF1α play a major role in the hypoxic response in mice as the lion's share of transcriptional response to hypoxia (i.e., up to 84%) in the liver is dependent on BMAL1 or HIF1α. The shared role of HIF1α and BMAL1 (∼50%) in the transcriptional responses to hypoxia is consistent with the finding that these bHLH-PAS domain-containing protein were reported to physically interact *in vitro*.[17,18,22] We also found independent roles for both these transcription factors in regulating the hypoxic response in a daytime-dependent manner, raising the possibility that HIF1α and BMAL1 could be part of different transcription factor complexes depending on the time of day. In this regard, HIF1α was shown to interact with several other clock proteins in cultured cells, such as PER1, PER2, CRY1, and CRY2.[19–21,61] Hence, it is feasible that depending on the time of day, the interacting partners of BMAL1 or HIF1α might differ and consequently activate different transcriptional programs in response to hypoxia. It would be, therefore, interesting to characterize these different complexes *in vivo* throughout the day.

We further found that in the liver, HIF1α accumulation upon hypoxia is temporally regulated and *Bmal1* dependent and that BMAL1 responds to hypoxia, in *Hif1α*-independent manner, likely through changes in its phosphorylation. It is still unclear whether the observed temporal changes in HIF1α accumulation as well as the effects on BMAL1 phosphorylation upon exposure of animals to hypoxia stem from a cell-autonomous response to low oxygen levels or are due to systemic effects. Cell culture assays are expected to shed light on these open questions.

Our experiments with BLKO mice clearly show that accumulation of HIF1α in the liver in response to hypoxia is *Bmal1* dependent. This is in line with a previous report that showed in cultured myotubes that the absence of *Bmal1* blunts HIF1α accumulation in response to hypoxia.[23] The molecular mechanisms that regulate HIF1α accumulation by *Bmal1* can occur at multiple levels and remain open for investigation. As we did not observe any major effect of *Bmal1* on *Hif1α* transcript levels upon hypoxia, it is conceivable that the effect of *Bmal1* on HIF1α accumulation is post-transcriptionally regulated. Along this line, HIF1α accumulation upon hypoxia is largely controlled post-transcriptionally through attenuation of its proteasomal degradation[62,63] raising the possibility that the BMAL1-HIF1α interaction might stabilize HIF1α, as was previously reported for HIF1β, which is vital for stabilization of HIF1α.[19,64]

Unexpectedly, we found that BHLKO mice exhibit reduced survival upon hypoxic exposure in a daytime-dependent manner. These mice rapidly die upon exposure to hypoxia in the subjective dark phase, whereas in the subjective light phase, they show high survival rates. One possible explanation is that these mice fail to compensate for the lack of oxygen when oxygen consumption is relatively high, as in the subjective dark phase when animals are active and consume food.[12]

The BHLKO mice exhibit characteristics of HPS; these include mild liver disease alongside hypoxemia and pulmonary vasodilation. The presence of this triad in BHLKO suggests that BMAL1 and HIF1α protect from HPS; however, the molecular mechanisms remain unknown. It should be pointed out that unlike CBD-induced HPS and often in HPS in humans, the alteration in liver functions is very mild in BHLKO mice. Nonetheless, these mice suffer from hypoxemia and pulmonary vasodilation. This raises the possibility that our genetic manipulation in the liver, namely hepatic knockout of *Bmal1* and *Hif1α*, is sufficient to affect lung function without inducing overt liver disease. The liver disease has been shown to exacerbate lung pathologies in HPS, which are ameliorated in humans upon liver transplantation.[65–68] This suggests that the liver-lung communication is critical for the disease progression and severity of HPS. Our BHLKO mice open exciting new avenues for the discovery of molecules that are implicated in liver-lung communication in general and specifically in the context of HPS.

In line with a previous report using CBDL-induced HPS,[49] we detected elevated levels of ET1 in the serum of BHLKO mice. Furthermore, our BHLKO liver transcriptome analyses pointed out major changes in *Serpina*, secreted serine protease inhibitors, which have been previously implicated in modulation of lung function.[59,60] Hence, it is tempting to speculate that these proteins might play a role in liver-lung communication in HIF1α- and BMAL1-dependent manner to modulate lung function. Having said that, inter-organ communication between the liver and the lung could be carried through a number of signaling molecules, which include as well small molecules such as metabolites or long non-coding RNAs,[69] and can be mediated through a third party, e.g., liver-gut-lung axis,[70–72] adding additional layers of complexity.

Hitherto, no genetic model in rodents is available for HPS, and future studies using BHLKO mice to investigate the pathophysiology of HPS are expected to provide new valuable information. As aforementioned, the currently available rodent model for studying HPS is through surgical intervention, namely CBDL.[73] Although this model has been informative,[38,39,73] it is often associated with high mortality rates, making it difficult to work with these diseased rodents.[74] Another major drawback of the CBDL model system is that bile duct ligation leads to the onset

(B) Proportion of a cell population relative to the total cells in the sample averaged across the three samples per genotype. Boxes reveal the average fraction of cells comprising the AlbCRE (gray) vs. the BHLKO (orange) lungs. The line in each box is at the mean. Multiple unpaired t tests (*$p < 0.05$).
(C–I) (C) The number of differentially expressed genes (DEGs) for each of the 12 major cell types (FDR< 0.05). Volcano plots reveal the up- (red) and downregulated (blue) DEGs for pseudobulked (D) endothelial cells, (E) stromal cells, and (F) alveolar macrophages with number of down- and upregulated genes in blue and red, respectively. Functional enrichment analysis reveals the top 10 Gene Ontology (GO) pathways (2–1,000 genes) ($p < 0.05$), which correspond to the DEGs of (G) endothelial cells, (H) stromal cells, and (I) alveolar macrophages.

of a severe liver disease that eventually causes the pulmonary vasodilation. However, in human studies, it has been established that HPS clearly occurs both in well-compensated and decompensated liver disease and also in situations where portal hypertension is present in the absence of cirrhosis.[38,39] Hence, our BHLKO mice are expected to serve as an attractive model for studying HPS, as these mice show characteristics of the syndrome in the presence of a very mild liver dysfunction.

In summary, our findings suggest that hepatic BMAL1 and HIF1α play a principal role in the transcriptional response to hypoxia and that their absence culminates in the development of HPS, potentially through the activation of eNOS, the accumulation of NO that induces pulmonary vasodilation and via modulation of the immune response. We propose that mice lacking *Bmal1* and *Hif1α* in the liver are an attractive genetic mouse model for studying HPS and offer a great opportunity to delineate HPS and related uncharted facets of liver-lung communication.

Limitations of the study

In this work, we show that a major part of the transcriptional response to hypoxia is mediated through BMAL1 and HIF1α in a time-dependent manner. We further show that BMAL1 is required for HIF1α accumulation upon hypoxia. However, at the molecular level, it remains unclear how BMAL1 supports HIF1α accumulation, and whether the observed changes in BMAL1 phosphorylation upon hypoxic exposure in mice are cell autonomous and a direct effect of hypoxia. Furthermore, we provide evidence that the absence of hepatic *Bmal1* and *Hif1α* results in the onset of hepatopulmonary-like syndrome in mice; however, the underlying molecular mechanism through which the liver communicates with the lung, in a *Bmal1*- and *Hif1α*-dependent manner, to modulate lung functions is lacking. We do show that the expression levels of several *Serpins* are altered in these liver-specific knockout mice, raising the possibility that they might be implicated in the process; however, their functional relevance needs to be tested.

STAR★METHODS

Detailed methods are provided in the online version of this paper and include the following:

SUPPLEMENTAL INFORMATION

Supplemental information can be found online at https://doi.org/10.1016/j.cmet.2024.07.003.

ACKNOWLEDGMENTS

We are grateful to Dr. Ori Brenner for his assistance with the analysis of the histological sections, Dr. Reinat Nevo for the image analyses, and all the members of the Asher lab for their comments on the manuscript. G.A. is supported by the European Research Council (ERC-2017 CIRCOMMUNICATION 770869), the Israel Science Foundation (ISF 1919/22), the Abisch Frenkel Foundation for the Promotion of Life Sciences, the Adelis Foundation, and Susan and Michael Stern. R.V.D. is supported by the US Fulbright program.

AUTHOR CONTRIBUTIONS

Conceptualization, V.D. and G.A.; investigation, V.D., N.B., R.V.D., G.M., H.B.-L., M.Z., I.K., M.G., and Y.A.; visualization, V.D.; data curation, V.D.; software, V.D.; funding, G.A.; writing–review & editing, V.D., N.B., and G.A.

DECLARATION OF INTERESTS

The authors declare no competing interests.

Received: January 29, 2024
Revised: May 28, 2024
Accepted: July 5, 2024
Published: August 5, 2024

REFERENCES

1. Bass, J., and Lazar, M.A. (2016). Circadian time signatures of fitness and disease. Science *354*, 994–999. https://doi.org/10.1126/science.aah4965.
2. Panda, S. (2016). Circadian physiology of metabolism. Science *354*, 1008–1015. https://doi.org/10.1126/science.aah4967.
3. Reinke, H., and Asher, G. (2019). Crosstalk between metabolism and circadian clocks. Nat. Rev. Mol. Cell Biol. *20*, 227–241. https://doi.org/10.1038/s41580-018-0096-9.
4. Bolshette, N., Ibrahim, H., Reinke, H., and Asher, G. (2023). Circadian regulation of liver function: from molecular mechanisms to disease pathophysiology. Nat. Rev. Gastroenterol. Hepatol. *20*, 695–707. https://doi.org/10.1038/s41575-023-00792-1.
5. Dibner, C., Schibler, U., and Albrecht, U. (2010). The mammalian circadian timing system: organization and coordination of central and peripheral clocks. Annu. Rev. Physiol. *72*, 517–549. https://doi.org/10.1146/annurev-physiol-021909-135821.
6. Patke, A., Young, M.W., and Axelrod, S. (2020). Molecular mechanisms and physiological importance of circadian rhythms. Nat. Rev. Mol. Cell Biol. *21*, 67–84. https://doi.org/10.1038/s41580-019-0179-2.
7. Takahashi, J.S. (2017). Transcriptional architecture of the mammalian circadian clock. Nat. Rev. Genet. *18*, 164–179. https://doi.org/10.1038/nrg.2016.150.
8. Zhang, E.E., and Kay, S.A. (2010). Clocks not winding down: unravelling circadian networks. Nat. Rev. Mol. Cell Biol. *11*, 764–776. https://doi.org/10.1038/nrm2995.
9. Adamovich, Y., Dandavate, V., and Asher, G. (2022). Circadian clocks' interactions with oxygen sensing and signalling. Acta Physiol. (Oxf.) *234*, e13770. https://doi.org/10.1111/apha.13770.
10. Peek, C.B. (2020). Metabolic implications of circadian-HIF crosstalk. Trends Endocrinol. Metab. *31*, 459–468. https://doi.org/10.1016/j.tem.2020.02.008.

11. O'Connell, E.J., Martinez, C.A., Liang, Y.G., Cistulli, P.A., and Cook, K.M. (2020). Out of breath, out of time: interactions between HIF and circadian rhythms. Am. J. Physiol. Cell Physiol. *319*, C533–C540. https://doi.org/10.1152/ajpcell.00305.2020.

12. Adamovich, Y., Ladeuix, B., Sobel, J., Manella, G., Neufeld-Cohen, A., Assadi, M.H., Golik, M., Kuperman, Y., Tarasiuk, A., Koeners, M.P., et al. (2019). Oxygen and carbon dioxide rhythms are circadian clock controlled and differentially directed by behavioral signals. Cell Metab. *29*, 1092–1103.e3. https://doi.org/10.1016/j.cmet.2019.01.007.

13. Adamovich, Y., Ladeuix, B., Golik, M., Koeners, M.P., and Asher, G. (2017). Rhythmic oxygen levels reset circadian clocks through HIF1alpha. Cell Metab. *25*, 93–101. https://doi.org/10.1016/j.cmet.2016.09.014.

14. Manella, G., Aviram, R., Bolshette, N., Muvkadi, S., Golik, M., Smith, D.F., and Asher, G. (2020). Hypoxia induces a time- and tissue-specific response that elicits intertissue circadian clock misalignment. Proc. Natl. Acad. Sci. USA *117*, 779–786. https://doi.org/10.1073/pnas.1914112117.

15. Manella, G., Ezagouri, S., Champigneulle, B., Gaucher, J., Mendelson, M., Lemarie, E., Stauffer, E., Pichon, A., Howe, C.A., Doutreleau, S., et al. (2022). The human blood transcriptome exhibits time-of-day-dependent response to hypoxia: lessons from the highest city in the world. Cell Rep. *40*, 111213. https://doi.org/10.1016/j.celrep.2022.111213.

16. Gabryelska, A., Turkiewicz, S., Karuga, F.F., Sochal, M., Strzelecki, D., and Białasiewicz, P. (2022). Disruption of circadian rhythm genes in obstructive sleep apnea patients-possible mechanisms involved and clinical implication. Int. J. Mol. Sci. *23*, 709. https://doi.org/10.3390/ijms23020709.

17. Takahata, S., Sogawa, K., Kobayashi, A., Ema, M., Mimura, J., Ozaki, N., and Fujii-Kuriyama, Y. (1998). Transcriptionally active heterodimer formation of an Arnt-like PAS protein, Arnt3, with HIF-1a, HLF, and clock. Biochem. Biophys. Res. Commun. *248*, 789–794. https://doi.org/10.1006/bbrc.1998.9012.

18. Hogenesch, J.B., Gu, Y.Z., Jain, S., and Bradfield, C.A. (1998). The basic-helix-loop-helix-PAS orphan MOP3 forms transcriptionally active complexes with circadian and hypoxia factors. Proc. Natl. Acad. Sci. USA *95*, 5474–5479. https://doi.org/10.1073/pnas.95.10.5474.

19. Chilov, D., Hofer, T., Bauer, C., Wenger, R.H., and Gassmann, M. (2001). Hypoxia affects expression of circadian genes PER1 and CLOCK in mouse brain. FASEB J. *15*, 2613–2622. https://doi.org/10.1096/fj.01-0092com.

20. Dimova, E.Y., Jakupovic, M., Kubaichuk, K., Mennerich, D., Chi, T.F., Tamanini, F., Oklejewicz, M., Hänig, J., Byts, N., Mäkelä, K.A., et al. (2019). The circadian clock protein CRY1 is a negative regulator of HIF-1α. iScience *13*, 284–304. https://doi.org/10.1016/j.isci.2019.02.027.

21. Vaughan, M.E., Wallace, M., Handzlik, M.K., Chan, A.B., Metallo, C.M., and Lamia, K.A. (2020). Cryptochromes suppress HIF1alpha in muscles. iScience *23*, 101338. https://doi.org/10.1016/j.isci.2020.101338.

22. Wu, Y., Tang, D., Liu, N., Xiong, W., Huang, H., Li, Y., Ma, Z., Zhao, H., Chen, P., Qi, X., et al. (2017). Reciprocal regulation between the circadian clock and hypoxia signaling at the genome level in mammals. Cell Metab. *25*, 73–85. https://doi.org/10.1016/j.cmet.2016.09.009.

23. Peek, C.B., Levine, D.C., Cedernaes, J., Taguchi, A., Kobayashi, Y., Tsai, S.J., Bonar, N.A., McNulty, M.R., Ramsey, K.M., and Bass, J. (2017). Circadian clock interaction with HIF1alpha mediates oxygenic metabolism and anaerobic glycolysis in skeletal muscle. Cell Metab. *25*, 86–92. https://doi.org/10.1016/j.cmet.2016.09.010.

24. Hogenesch, J.B., Chan, W.K., Jackiw, V.H., Brown, R.C., Gu, Y.Z., Pray-Grant, M., Perdew, G.H., and Bradfield, C.A. (1997). Characterization of a subset of the basic-helix-loop-helix-PAS superfamily that interacts with components of the dioxin signaling pathway. J. Biol. Chem. *272*, 8581–8593. https://doi.org/10.1074/jbc.272.13.8581.

25. Koike, N., Yoo, S.H., Huang, H.C., Kumar, V., Lee, C., Kim, T.K., and Takahashi, J.S. (2012). Transcriptional architecture and chromatin landscape of the core circadian clock in mammals. Science *338*, 349–354. https://doi.org/10.1126/science.1226339.

26. Menet, J.S., Pescatore, S., and Rosbash, M. (2014). CLOCK:BMAL1 is a pioneer-like transcription factor. Genes Dev. *28*, 8–13. https://doi.org/10.1101/gad.228536.113.

27. Rey, G., Cesbron, F., Rougemont, J., Reinke, H., Brunner, M., and Naef, F. (2011). Genome-wide and phase-specific DNA-binding rhythms of BMAL1 control circadian output functions in mouse liver. PLoS Biol. *9*, e1000595. https://doi.org/10.1371/journal.pbio.1000595.

28. Semenza, G.L. (2001). HIF-1 and mechanisms of hypoxia sensing. Curr. Opin. Cell Biol. *13*, 167–171. https://doi.org/10.1016/s0955-0674(00)00194-0.

29. Lamia, K.A., Storch, K.F., and Weitz, C.J. (2008). Physiological significance of a peripheral tissue circadian clock. Proc. Natl. Acad. Sci. USA *105*, 15172–15177. https://doi.org/10.1073/pnas.0806717105.

30. Manella, G., Sabath, E., Aviram, R., Dandavate, V., Ezagouri, S., Golik, M., Adamovich, Y., and Asher, G. (2021). The liver-clock coordinates rhythmicity of peripheral tissues in response to feeding. Nat. Metab. *3*, 829–842. https://doi.org/10.1038/s42255-021-00395-7.

31. Ryan, H.E., Poloni, M., McNulty, W., Elson, D., Gassmann, M., Arbeit, J.M., and Johnson, R.S. (2000). Hypoxia-inducible factor-1alpha is a positive factor in solid tumor growth. Cancer Res. *60*, 4010–4015.

32. Tajima, T., Goda, N., Fujiki, N., Hishiki, T., Nishiyama, Y., Senoo-Matsuda, N., Shimazu, M., Soga, T., Yoshimura, Y., Johnson, R.S., et al. (2009). HIF-1alpha is necessary to support gluconeogenesis during liver regeneration. Biochem. Biophys. Res. Commun. *387*, 789–794. https://doi.org/10.1016/j.bbrc.2009.07.115.

33. Button, E.L., Bersten, D.C., and Whitelaw, M.L. (2017). HIF has Biff - cross-talk between HIF1a and the family of bHLH/PAS proteins. Exp. Cell Res. *356*, 141–145. https://doi.org/10.1016/j.yexcr.2017.03.055.

34. Kasarala, G., and Tillmann, H.L. (2016). Standard liver tests. Clin. Liver Dis. (Hoboken) *8*, 13–18. https://doi.org/10.1002/cld.562.

35. Manni, I., Di Rocco, G., Fusco, S., Leone, L., Barbati, S.A., Carapella, C.M., Grassi, C., Piaggio, G., and Toietta, G. (2016). Monitoring the response of hyperbilirubinemia in the mouse brain by in vivo bioluminescence imaging. Int. J. Mol. Sci. *18*, 50. https://doi.org/10.3390/ijms18010050.

36. Abd El-Ghffar, E.A., El-Nashar, H.A.S., Eldahshan, O.A., and Singab, A.N.B. (2017). GC-MS analysis and hepatoprotective activity of the n-hexane extract of Acrocarpus fraxinifolius leaves against paracetamol-induced hepatotoxicity in male albino rats. Pharm. Biol. *55*, 441–449. https://doi.org/10.1080/13880209.2016.1246575.

37. Gounden, V., Bhatt, H., and Jialal, I. (2024). Renal function tests. In StatPearls (StatPearls Publishing).

38. Raevens, S., Boret, M., and Fallon, M.B. (2022). Hepatopulmonary syndrome. JHEP Rep. *4*, 100527. https://doi.org/10.1016/j.jhepr.2022.100527.

39. Zhang, J., and Fallon, M.B. (2012). Hepatopulmonary syndrome: update on pathogenesis and clinical features. Nat. Rev. Gastroenterol. Hepatol. *9*, 539–549. https://doi.org/10.1038/nrgastro.2012.123.

40. Iversen, N.K., Malte, H., Baatrup, E., and Wang, T. (2012). The normal acid-base status of mice. Respir. Physiol. Neurobiol. *180*, 252–257. https://doi.org/10.1016/j.resp.2011.11.015.

41. Abrams, G.A., Jaffe, C.C., Hoffer, P.B., Binder, H.J., and Fallon, M.B. (1995). Diagnostic utility of contrast echocardiography and lung perfusion scan in patients with hepatopulmonary syndrome. Gastroenterology *109*, 1283–1288. https://doi.org/10.1016/0016-5085(95)90589-8.

42. Aller, R., Moya, J.L., Moreira, V., Boixeda, D., Cano, A., Picher, J., García-Rull, S., and de Luis, D.A. (1999). Diagnosis of hepatopulmonary syndrome with contrast transesophageal echocardiography: advantages over contrast transthoracic echocardiography. Dig. Dis. Sci. *44*, 1243–1248. https://doi.org/10.1023/a:1026657114256.

43. Bansal, K., Gore, M., and Mittal, S. (2023). Hepatopulmonary syndrome. In StatPearls (StatPearls Publishing).

44. Serres, F., Chetboul, V., Tissier, R., Gouni, V., Desmyter, A., Sampedrano, C.C., and Pouchelon, J.L. (2009). Quantification of pulmonary to systemic

flow ratio by a Doppler echocardiographic method in the normal dog: repeatability, reproducibility, and reference ranges. J. Vet. Cardiol. *11*, 23–29. https://doi.org/10.1016/j.jvc.2009.04.001.

45. Vargas Barron, J., Sahn, D.J., Valdes-Cruz, L.M., Lima, C.O., Goldberg, S.J., Grenadier, E., and Allen, H.D. (1984). Clinical utility of two-dimensional doppler echocardiographic techniques for estimating pulmonary to systemic blood flow ratios in children with left to right shunting atrial septal defect, ventricular septal defect or patent ductus arteriosus. J. Am. Coll. Cardiol. *3*, 169–178. https://doi.org/10.1016/s0735-1097(84)80445-3.

46. Tran, N., Garcia, T., Aniqa, M., Ali, S., Ally, A., and Nauli, S.M. (2022). Endothelial nitric oxide synthase (eNOS) and the cardiovascular system: in physiology and in disease states. Am. J. Biomed. Sci. Res. *15*, 153–177.

47. Martin, P.Y., Xu, D.L., Niederberger, M., Weigert, A., Tsai, P., St John, J., Gines, P., and Schrier, R.W. (1996). Upregulation of endothelial constitutive NOS: a major role in the increased NO production in cirrhotic rats. Am. J. Physiol. *270*, F494–F499. https://doi.org/10.1152/ajprenal.1996.270.3.F494.

48. Zhang, M., Luo, B., Chen, S.J., Abrams, G.A., and Fallon, M.B. (1999). Endothelin-1 stimulation of endothelial nitric oxide synthase in the pathogenesis of hepatopulmonary syndrome. Am. J. Physiol. *277*, G944–G952. https://doi.org/10.1152/ajpgi.1999.277.5.G944.

49. Ling, Y., Zhang, J., Luo, B., Song, D., Liu, L., Tang, L., Stockard, C.R., Grizzle, W.E., Ku, D.D., and Fallon, M.B. (2004). The role of endothelin-1 and the endothelin B receptor in the pathogenesis of hepatopulmonary syndrome in the rat. Hepatology *39*, 1593–1602. https://doi.org/10.1002/hep.20244.

50. Fulton, D., Gratton, J.P., McCabe, T.J., Fontana, J., Fujio, Y., Walsh, K., Franke, T.F., Papapetropoulos, A., and Sessa, W.C. (1999). Regulation of endothelium-derived nitric oxide production by the protein kinase Akt. Nature *399*, 597–601. https://doi.org/10.1038/21218.

51. Wu, M., Komori, N., Qin, C., Farber, J.P., Linderoth, B., and Foreman, R.D. (2008). Extracellular signal-regulated kinase (ERK) and protein kinase B (AKT) pathways involved in spinal cord stimulation (SCS)-induced vasodilation. Brain Res. *1207*, 73–83. https://doi.org/10.1016/j.brainres.2007.12.072.

52. Yang, W., Zhang, J., Hu, B., Wu, W., Venter, J., Alpini, G., and Fallon, M.B. (2014). The role of receptor tyrosine kinase activation in cholangiocytes and pulmonary vascular endothelium in experimental hepatopulmonary syndrome. Am. J. Physiol. Gastrointest. Liver Physiol. *306*, G72–G80. https://doi.org/10.1152/ajpgi.00178.2013.

53. Zhang, J., Luo, B., Tang, L., Wang, Y., Stockard, C.R., Kadish, I., Van Groen, T., Grizzle, W.E., Ponnazhagan, S., and Fallon, M.B. (2009). Pulmonary angiogenesis in a rat model of hepatopulmonary syndrome. Gastroenterology *136*, 1070–1080. https://doi.org/10.1053/j.gastro.2008.12.001.

54. Guo, M., Morley, M.P., Jiang, C., Wu, Y., Li, G., Du, Y., Zhao, S., Wagner, A., Cakar, A.C., Kouril, M., et al. (2023). Guided construction of single cell reference for human and mouse lung. Nat. Commun. *14*, 4566. https://doi.org/10.1038/s41467-023-40173-5.

55. Koenitzer, J.R., Wu, H., Atkinson, J.J., Brody, S.L., and Humphreys, B.D. (2020). Single-nucleus RNA-sequencing profiling of mouse lung. reduced dissociation bias and improved rare cell-type detection compared with single-cell RNA sequencing. Am. J. Respir. Cell Mol. Biol. *63*, 739–747. https://doi.org/10.1165/rcmb.2020-0095MA.

56. Delaney, C., Davizon-Castillo, P., Allawzi, A., Posey, J., Gandjeva, A., Neeves, K., Tuder, R.M., Di Paola, J., Stenmark, K.R., and Nozik, E.S. (2021). Platelet activation contributes to hypoxia-induced inflammation. Am. J. Physiol. Lung Cell. Mol. Physiol. *320*, L413–L421. https://doi.org/10.1152/ajplung.00519.2020.

57. Middleton, E.A., Weyrich, A.S., and Zimmerman, G.A. (2016). Platelets in pulmonary immune responses and inflammatory lung diseases. Physiol. Rev. *96*, 1211–1259. https://doi.org/10.1152/physrev.00038.2015.

58. Shen, Z., Wei, L., Yu, Z.B., Yao, Z.Y., Cheng, J., Wang, Y.T., Song, X.T., and Li, M. (2021). The roles of TRIMs in antiviral innate immune signaling. Front. Cell. Infect. Microbiol. *11*, 628275. https://doi.org/10.3389/fcimb.2021.628275.

59. Bashir, A., Shah, N.N., Hazari, Y.M., Habib, M., Bashir, S., Hilal, N., Banday, M., Asrafuzzaman, S., and Fazili, K.M. (2016). Novel variants of SERPIN1A gene: interplay between alpha1-antitrypsin deficiency and chronic obstructive pulmonary disease. Respir. Med. *117*, 139–149. https://doi.org/10.1016/j.rmed.2016.06.005.

60. Jezela-Stanek, A., and Chorostowska-Wynimko, J. (2023). SERPINA1 and more? A putative genetic contributor to pulmonary dysfunction in alpha-1 antitrypsin deficiency. J. Clin. Med. *12*, 1708. https://doi.org/10.3390/jcm12051708.

61. Kobayashi, M., Morinibu, A., Koyasu, S., Goto, Y., Hiraoka, M., and Harada, H. (2017). A circadian clock gene, PER2, activates HIF-1 as an effector molecule for recruitment of HIF-1alpha to promoter regions of its downstream genes. FEBS Journal *284*, 3804–3816. https://doi.org/10.1111/febs.14280.

62. Semenza, G.L. (2001). Hypoxia-inducible factor 1: oxygen homeostasis and disease pathophysiology. Trends Mol. Med. *7*, 345–350. https://doi.org/10.1016/s1471-4914(01)02090-1.

63. Mole, D.R., Maxwell, P.H., Pugh, C.W., and Ratcliffe, P.J. (2001). Regulation of HIF by the Von Hippel-Lindau tumour suppressor: implications for cellular oxygen sensing. IUBMB Life *52*, 43–47. https://doi.org/10.1080/15216540252774757.

64. Berra, E., Roux, D., Richard, D.E., and Pouysségur, J. (2001). Hypoxia-inducible factor-1 alpha (HIF-1 alpha) escapes O(2)-driven proteasomal degradation irrespective of its subcellular localization: nucleus or cytoplasm. EMBO Rep. *2*, 615–620. https://doi.org/10.1093/embo-reports/kve130.

65. Arguedas, M.R., Abrams, G.A., Krowka, M.J., and Fallon, M.B. (2003). Prospective evaluation of outcomes and predictors of mortality in patients with hepatopulmonary syndrome undergoing liver transplantation. Hepatology *37*, 192–197. https://doi.org/10.1053/jhep.2003.50023.

66. Arguedas, M.R., Singh, H., Faulk, D.K., and Fallon, M.B. (2007). Utility of pulse oximetry screening for hepatopulmonary syndrome. Clin. Gastroenterol. Hepatol. *5*, 749–754. https://doi.org/10.1016/j.cgh.2006.12.003.

67. Fallon, M.B., Krowka, M.J., Brown, R.S., Trotter, J.F., Zacks, S., Roberts, K.E., Shah, V.H., Kaplowitz, N., Forman, L., Wille, K., et al. (2008). Impact of hepatopulmonary syndrome on quality of life and survival in liver transplant candidates. Gastroenterology *135*, 1168–1175. https://doi.org/10.1053/j.gastro.2008.06.038.

68. Krowka, M.J., and Cortese, D.A. (1990). Hepatopulmonary syndrome: an evolving perspective in the era of liver transplantation. Hepatology *11*, 138–142. https://doi.org/10.1002/hep.1840110123.

69. Yang, C., Yang, Y., Chen, Y., Huang, J., Li, D., Tang, X., Ning, J., Gu, J., Yi, B., and Lu, K. (2024). Cholangiocyte-derived exosomal long noncoding RNA PICALM-AU1 promotes pulmonary endothelial cell endothelial-mesenchymal transition in hepatopulmonary syndrome. Heliyon *10*, e24962. https://doi.org/10.1016/j.heliyon.2024.e24962.

70. Zhang, H.Y., Han, D.W., Wang, X.G., Zhao, Y.C., Zhou, X., and Zhao, H.Z. (2005). Experimental study on the role of endotoxin in the development of hepatopulmonary syndrome. World J. Gastroenterol. *11*, 567–572. https://doi.org/10.3748/wjg.v11.i4.567.

71. Sztrymf, B., Libert, J.M., Mougeot, C., Lebrec, D., Mazmanian, M., Humbert, M., and Herve, P. (2005). Cirrhotic rats with bacterial translocation have higher incidence and severity of hepatopulmonary syndrome. J. Gastroenterol. Hepatol. *20*, 1538–1544. https://doi.org/10.1111/j.1440-1746.2005.03914.x.

72. Schroeder, R.A., Ewing, C.A., Sitzmann, J.V., and Kuo, P.C. (2000). Pulmonary expression of iNOS and HO-1 protein is upregulated in a rat model of prehepatic portal hypertension. Dig. Dis. Sci. *45*, 2405–2410. https://doi.org/10.1023/a:1005651327654.

73. Fallon, M.B., Abrams, G.A., McGrath, J.W., Hou, Z., and Luo, B. (1997). Common bile duct ligation in the rat: a model of intrapulmonary

vasodilatation and hepatopulmonary syndrome. Am. J. Physiol. *272*, G779–G784. https://doi.org/10.1152/ajpgi.1997.272.4.G779.

74. Yang, Y., Chen, B., Chen, Y., Zu, B., Yi, B., and Lu, K. (2015). A comparison of two common bile duct ligation methods to establish hepatopulmonary syndrome animal models. Lab Anim. *49*, 71–79. https://doi.org/10.1177/0023677214558701.
75. Asher, G., Reinke, H., Altmeyer, M., Gutierrez-Arcelus, M., Hottiger, M.O., and Schibler, U. (2010). Poly(ADP-ribose) polymerase 1 participates in the phase entrainment of circadian clocks to feeding. Cell *142*, 943–953. https://doi.org/10.1016/j.cell.2010.08.016.
76. Arganda-Carreras, I., Kaynig, V., Rueden, C., Eliceiri, K.W., Schindelin, J., Cardona, A., and Sebastian Seung, H. (2017). Trainable Weka segmentation: a machine learning tool for microscopy pixel classification. Bioinformatics *33*, 2424–2426. https://doi.org/10.1093/bioinformatics/btx180.
77. Kohen, R., Barlev, J., Hornung, G., Stelzer, G., Feldmesser, E., Kogan, K., Safran, M., and Leshkowitz, D. (2019). UTAP: user-friendly transcriptome analysis pipeline. BMC Bioinformatics *20*, 154. https://doi.org/10.1186/s12859-019-2728-2.
78. Chen, E.Y., Tan, C.M., Kou, Y., Duan, Q., Wang, Z., Meirelles, G.V., Clark, N.R., and Ma'ayan, A. (2013). Enrichr: interactive and collaborative HTML5 gene list enrichment analysis tool. BMC Bioinformatics *14*, 128. https://doi.org/10.1186/1471-2105-14-128.
79. Butler, A., Hoffman, P., Smibert, P., Papalexi, E., and Satija, R. (2018). Integrating single-cell transcriptomic data across different conditions, technologies, and species. Nat. Biotechnol. *36*, 411–420. https://doi.org/10.1038/nbt.4096.
80. Becht, E., McInnes, L., Healy, J., Dutertre, C.-A., Kwok, I.W.H., Ng, L.G., Ginhoux, F., and Newell, E.W. (2019). Dimensionality reduction for visualizing single-cell data using UMAP. Nat. Biotechnol. *37*, 38–44. https://doi.org/10.1038/nbt.4314.
81. Aran, D., Looney, A.P., Liu, L., Wu, E., Fong, V., Hsu, A., Chak, S., Naikawadi, R.P., Wolters, P.J., Abate, A.R., et al. (2019). Reference-based analysis of lung single-cell sequencing reveals a transitional profibrotic macrophage. Nat. Immunol. *20*, 163–172. https://doi.org/10.1038/s41590-018-0276-y.
82. Aviram, R., Manella, G., Kopelman, N., Neufeld-Cohen, A., Zwighaft, Z., Elimelech, M., Adamovich, Y., Golik, M., Wang, C., Han, X., and Asher, G. (2016). Lipidomics analyses reveal temporal and spatial lipid organization and uncover daily oscillations in intracellular organelles. Mol. Cell *62*, 636–648. https://doi.org/10.1016/j.molcel.2016.04.002.
83. Lavery, D.J., and Schibler, U. (1993). Circadian transcription of the cholesterol 7 alpha hydroxylase gene may involve the liver-enriched bZIP protein DBP. Genes Dev. *7*, 1871–1884. https://doi.org/10.1101/gad.7.10.1871.
84. Jaitin, D.A., Kenigsberg, E., Keren-Shaul, H., Elefant, N., Paul, F., Zaretsky, I., Mildner, A., Cohen, N., Jung, S., Tanay, A., et al. (2014). Massively parallel single-cell RNA-seq for marker-free decomposition of tissues into cell types. Science *343*, 776–779. https://doi.org/10.1126/science.1247651.
85. Dobin, A., Davis, C.A., Schlesinger, F., Drenkow, J., Zaleski, C., Jha, S., Batut, P., Chaisson, M., and Gingeras, T.R. (2013). STAR: ultrafast universal RNA-seq aligner. Bioinformatics *29*, 15–21. https://doi.org/10.1093/bioinformatics/bts635.
86. Anders, S., Pyl, P.T., and Huber, W. (2015). HTSeq–a Python framework to work with high-throughput sequencing data. Bioinformatics *31*, 166–169. https://doi.org/10.1093/bioinformatics/btu638.
87. Love, M.I., Huber, W., and Anders, S. (2014). Moderated estimation of fold change and dispersion for RNA-seq data with DESeq2. Genome Biol. *15*, 550. https://doi.org/10.1186/s13059-014-0550-8.
88. Anders, S., and Huber, W. (2010). Differential expression analysis for sequence count data. Genome Biol. *11*, R106. https://doi.org/10.1186/gb-2010-11-10-r106.
89. Schindelin, J., Arganda-Carreras, I., Frise, E., Kaynig, V., Longair, M., Pietzsch, T., Preibisch, S., Rueden, C., Saalfeld, S., Schmid, B., et al. (2012). Fiji: an open-source platform for biological-image analysis. Nat. Methods *9*, 676–682. https://doi.org/10.1038/nmeth.2019.
90. Hao, Y., Hao, S., Andersen-Nissen, E., Mauck, W.M., 3rd, Zheng, S., Butler, A., Lee, M.J., Wilk, A.J., Darby, C., Zager, M., et al. (2021). Integrated analysis of multimodal single-cell data. Cell *184*, 3573–3587.e29. https://doi.org/10.1016/j.cell.2021.04.048.
91. Squair, J.W., Gautier, M., Kathe, C., Anderson, M.A., James, N.D., Hutson, T.H., Hudelle, R., Qaiser, T., Matson, K.J.E., Barraud, Q., et al. (2021). Confronting false discoveries in single-cell differential expression. Nat. Commun. *12*, 5692. https://doi.org/10.1038/s41467-021-25960-2.
92. Ge, S.X., Jung, D., and Yao, R. (2020). ShinyGO: a graphical gene-set enrichment tool for animals and plants. Bioinformatics *36*, 2628–2629. https://doi.org/10.1093/bioinformatics/btz931.

Please cite this article in press as: Dandavate et al., Hepatic BMAL1 and HIF1α regulate a time-dependent hypoxic response and prevent hepatopulmonary-like syndrome, Cell Metabolism (2024), https://doi.org/10.1016/j.cmet.2024.07.003

CellPress

STAR★METHODS

KEY RESOURCES TABLE

REAGENT or RESOURCE	SOURCE	IDENTIFIER
Antibodies		
Rabbit anti-HIF1A	Cell Signaling Technology	D1S7W; RRID: AB_2799095
Rabbit anti-BMAL1	Asher et al.[75]	N/A
Mouse anti-eNOS	Santa Cruz Biotechnology	376751; RRID: AB_2832203
Rabbit anti-ERK	Sigma Aldrich	M5670; RRID: AB_477216
Rabbit anti-pERK	Cell Signaling Technology	9101; RRID: AB_331646
Rabbit anti-pAKT (Ser473)	Cell Signaling Technology	4060; RRID: AB_329825
Rabbit anti-AKT (PAN)	Cell Signaling Technology	2920; RRID: AB_1147620
Rabbit anti-iNOS	Thermo Fisher Scientific	PA3-030A; RRID: AB_2152737
Mouse anti-Endothelin 1	Abcam	ab2786; RRID: AB_303299
PCNA (PC10) Mouse	Cell Signaling Technology	2586; RRID: AB_2160343
Mouse anti-TUBULIN	Sigma Aldrich	T9026; RRID: AB_477593
Mouse anti-ACTIN	Sigma Aldrich	A3853; RRID: AB_262137
Mouse anti-U2AF	Sigma Aldrich	U4758; RRID: AB_262122
Anti-mouse secondary antibody	Jackson ImmunoResearch	115-035-146
Anti-rabbit secondary antibody	Jackson ImmunoResearch	111-035-144
Chemicals, peptides, and recombinant proteins		
TRI reagent	Sigma Aldrich	T9424
LightCycler 480 Syber Green I Master	Roche Applied Science	04887352001
Protease Inhibitors Cocktail Set III	EMD - MERCK MILLIPORE	539134
Paraformaldehyde	Santa Cruz Biotechnology	sc-281692
Vevo MicroMarker Non-Targeted Contrast Agent Kit	ELSMED	#1193
Haematoxylin Gill II Eosin Y (alcoholic solution)	Leica	380152E
Critical commercial assays		
qScript cDNA synthesis kit	Quanta Biosciences	95047-100
Bradford assay	Bio-Rad Laboratories	500-0006
Nitric Oxide Assay Kit	Abcam	ab272517
Miltenyi Biotec lung dissociation kit	Miltenyi Biotec	130-095-927
Chromium Single Cell 3' Reagent Kits v3.1 protocol	10x Chromium	CG000204
Chromium Next GEM Chip G	10x Chromium	PN-1000120
Chromium Single Cell 3' GEM, Library & Gel Bead Kit v3	10x Chromium	PN-1000121
Agilent High Sensitive DNA Kit	Agilent Technologies	5067—4626
Illumina Novaseq System	Illumina	NovaSeq 6000
Proteome Profiler Mouse Cytokine Array Kit	R and D Systems - Bio-Techne Corp 486	ARY006
Triglyceride Colorimetric Assay Kit	Cayman Chemical	10010303
Deposited data		
RNA-Seq (livers)	Gene Expression omnibus database (GEO)	GEO: GSE254438
RNA-Seq (lungs)	Gene Expression omnibus database (GEO)	GEO: GSE254219
Single-cell RNA-Seq	Gene Expression omnibus database (GEO)	GEO: GSE266410
Data S1	Raw data files	Data S1

(*Continued on next page*)

Please cite this article in press as: Dandavate et al., Hepatic BMAL1 and HIF1α regulate a time-dependent hypoxic response and prevent hepatopulmonary-like syndrome, Cell Metabolism (2024), https://doi.org/10.1016/j.cmet.2024.07.003

Continued

REAGENT or RESOURCE	SOURCE	IDENTIFIER
Experimental models: Organisms/strains		
AlbCre^{+} mice	Jackson Laboratories	003574
Bmal1$^{fl/fl}$ mice	Jackson Laboratories	007668
Hif1α$^{fl/fl}$ mice	Jackson Laboratories	007561
Oligonucleotides		
Primers for real-time PCR are listed in Table S3	Supplemental information in the current paper	N/A
Software and algorithms		
R (version 4.2.1)	CRAN	N/A
ggplot2	CRAN	N/A
ImageJ	Open source	https://imagej.net/software/fiji/
Trainable Weka Segmentation	Arganda-Carreras et al.[76]	https://imagej.net/plugins/tws/
GraphPad Prism (version 10.2.2)	Dotmatics	https://www.graphpad.com/how-to-buy/
DESeq2 (version 1.24.0)	Bioconductor	https://bioconductor.org/packages/release/bioc/html/DESeq2.html
UTAP	Kohen et al.[77]	N/A
EnrichR	Chen et al.[78]	N/A
Vevo Lab software (version 5.8.1)	FUJIFILM VisualSonics	N/A
Biorender	BioRender.com	N/A
Cell Ranger	10X Genomics	N/A
Seurat_4.1.0	Butler et al.[79]	N/A
Uniform Manifold Approximation and Projection (UMAP)	Becht et al.[80]	N/A
SingleR	Aran et al.[81]	N/A
Others		
CG4+ cartridges	Abbott	ABT-03P85-25
Regular chow- Teklad Global 18% Protein Rodent Diet	Teklad Diets	2018
VELO2x	Baker Co	N/A
VetScan i-STAT 1 analyser	Abaxix	N/A

RESOURCE AVAILABILITY

Lead contact

Further information and requests for resources and reagents should be directed to and will be fulfilled by the Lead Contact, Gad Asher (gad.asher@weizmann.ac.il)

Materials availability

This study did not generate new unique reagents.

Data and code availability

- RNA-seq data, including fastq files and raw counts have been deposited at GEO and are publicly available as of the date of publication. Accession numbers are listed in the key resources table. Data S1 contains unprocessed source data underlying all blots and graphs
- This paper does not report original code.
- Any additional information required to reanalyze the data reported in this paper is available from the lead contact upon request.

EXPERIMENTAL MODEL AND STUDY PARTICIPANT DETAILS

Animals

All animal experiments and procedures were conducted in conformity and approval of the Weizmann Institute Animal Care and Use Committee (IACUC). Three to four months-old male mice were used. *AlbCre*$^{+}$ *Bmal1*$^{fl/fl}$ (BLKO), *AlbCre*$^{+}$ *Hif1α*$^{fl/fl}$ (HLKO) and *AlbCre*$^{+}$

Bmal1$^{fl/fl}$ *Hif1α*$^{fl/f}$ (BHLKO) were generated by crossing *AlbCre*$^{+}$ mice with *Bmal1*$^{fl/fl}$ mice, *Hif1α*$^{fl/fl}$ and *Bmal1*$^{fl/fl}$, *Hif1α*$^{fl/fl}$ (Jackson Laboratories). Animals were housed in an SPF animal facility, at room temperature of ≈ 22°C, under a 12 h light-dark regimen (LD) and fed *ad libitum*. Experiments were performed in constant dark (DD). Lights were turned off at the transition of dark to light regimen on the day of the experiment, following regular LD regimen. Mice were euthanized by cervical dislocation.

METHOD DETAILS

Hypoxia *in vivo*

The hypoxic exposure was conducted using the VelO$_2$x *in vivo* hypoxia system (Baker Co.). Oxygen levels were gradually decreased from 21% oxygen to 6% oxygen within 5' in exchange of nitrogen and sustained at 6% oxygen for the indicted time. Mortality in response to hypoxia was assessed upon 30min or 4h hypoxic exposure in separate experiments as we had to open the VelO$_2$x chamber to determine mortality.

RNA extraction and Quantitative PCR

Tissues were snap-frozen in liquid nitrogen immediately after dissection and stored at −80°C for further use. For RNA extraction, the samples were soaked in TRI-reagent (Sigma) and were homogenized by Bead mill homogenizer (OMNI International), and then proceeded by a standard TRI-reagent based RNA extraction protocol. RNA concentration was determined using a NanoDrop 2000 Spectrophotometer (Thermo Fisher Scientific). RNA quality was validated using 2200 TapeStation (Agilent). Synthesis of cDNA was performed using qScript cDNA SuperMix (Quanta Biosciences). Real-time quantitative PCR measurements were performed using SYBR Green with a LightCycler II machine (Roche) and normalized to the geometric mean of three housekeeping genes: we used *Tbp*, *Gapdh*, and *Actin* for the liver and *Hprt*, *Rplp0* and *Gapdh* for the lung. Primers are listed in Table S3.

Protein extraction and Immunoblot analysis

Samples were snap-frozen in liquid nitrogen immediately after dissection and stored at −80°C until use. For total protein extraction, tissues were homogenized by Bead mill homogenizer (OMNI International) in ice-cold RIPA buffer (150 mM NaCl, 1% NP-40, 0.5% Na-deoxycholate, 0.1% SDS, 50 mM Tris-Hcl pH 8, and 1 mM dithiothreitol). The extracts were centrifuged at 21,000 g for 30 min at 4°C.

Nuclei from tissues were isolated by density sucrose gradient as previously described.[82] The entire liver was homogenized using an IKA douncer, in 4 ml 0.3 M sucrose homogenization buffer (10 mM Hepes pH 7.6, 15 mM KCl, 2 mM EDTA, 0.15 mM spermine, 0.5 mM spermidine, 10% glycerol), and 7 ml of 2.2 M sucrose homogenization buffer (10 mM Hepes pH 7.6, 15 mM KCl, 2 mM EDTA 0.2 M, 0.15 mM spermine, 0.5 mM spermidine, 10% glycerol). Following homogenization, 18 ml of 2.2 M homogenization buffer were added, and samples were transferred to a 10 ml Cushion sucrose buffer 2.05 M (10 mM Hepes pH 7.6, 15 mM KCl, 2 mM EDTA, 0.15 mM spermine, 0.5 mM spermidine, 10% glycerol) and centrifuged for 1 h, 24,000 rpm, 4°C. Pellet was suspended in isotonic buffer (10 mM Hepes pH 7.6, 100 mM KCl, 0.15 mM spermine, 0.5 mM spermidine, 10% Glycerol). Subsequently the nuclear proteins were extracted by adding 1:1 NUN buffer (50mM HEPES pH=7.6, 0.6M NaCl, 2% NP-40, 2M Urea).[83] All buffers were supplemented with protease inhibitors cocktail (Protease Inhibitor Cocktail Set III, EDTA-Free, EMD Millipore Corp, 539134), PMSF (1:200), vanadate (1:500), DTT (1:1000), NaF (1:1000).

Protein concentration was determined by the Bradford assay (Bio-Rad) and normalized between samples. Then, samples were heated at 95°C for 5 min in Laemmli sample buffer and analyzed by SDS-PAGE and immunoblot. Antibodies that were used: Rabbit anti-BMAL1 (Asher et al., 2010), Rabbit anti-HIF1A (Cell Signaling, D1S7W), Mouse anti-eNOS (Santa Cruz, 376751), Rabbit anti-ERK (Sigma Aldrich, M5670), Rabbit anti-pERK (Cell Signaling Technology, 9101), Rabbit anti-pAKT (Cell Signaling Technology, 4060), Rabbit anti-AKT (PAN) (Cell Signaling Technology, 2920), Rabbit anti-iNOS (ThermoFisher Scientific, PA3-030A), Mouse anti-TUBULIN (Sigma, T9026), Mouse anti-ACTIN (Sigma, A3853), Mouse anti-Endothelin 1 (Abcam, ab2786), Mouse anti-PCNA (Cell Signaling Technology, 2586) and Mouse anti-U2AF (Sigma, U4758).

Mouse Cytokine Array

Mouse serum from each genotype was obtained at CT16 normoxia and pooled together (n=5). 120μl of pooled serum were analyzed in duplicates using Mouse Cytokine Array Panel A (ARY006) according to the manufacturer's protocol. The pixel densities of each cytokine were quantified for the different genotypes with image analysis software (ImageJ). Only cytokines with mean pixel density value more than 1000 in at least one genotype were included in the analysis.

Liver Triglycerides measurements

Triglyceride levels in the mouse livers were determined using the Triglyceride Colorimetric Assay Kit (Cayman Chemical, 10010303) according to the protocol supplied by the manufacturer.

MARS-seq library preparation and sequencing

We used a derivation of the MARS-seq as described,[84] originally developed for singlecell RNA-seq to produce expression libraries, and exclusively sequencing the 3'-end of the transcripts. The prepared MARS-seq libraries were sequenced with high-output 75 bp kit (NextSeq 500/550 High Output Kit v2.5 (75 Cycles) 20024906, Illumina) on NextSeq 500/550 Illumina sequencer.

Please cite this article in press as: Dandavate et al., Hepatic BMAL1 and HIF1α regulate a time-dependent hypoxic response and prevent hepatopulmonary-like syndrome, Cell Metabolism (2024), https://doi.org/10.1016/j.cmet.2024.07.003

RNA-seq data processing of raw sequencing data into read counts was performed via the User-friendly Transcriptome Analysis Pipeline (UTAP).[77] In short, reads were trimmed using cutadapt and mapped to genome (/shareDB/iGenomes/Mus_musculus/UCSC/mm10/Sequence/ STAR_index) using STAR[85] (default parameters). The pipeline quantifies the genes annotated in RefSeq (that have expanded with 1000 bases toward 5' edge and 100 bases toward 3' bases). Counting was done using htseq-count (union mode).[86] RNA-seq statistical analysis was performed together for all genotypes. Only genes with minimum 5 read in at least one sample were included in the analysis. The data was normalized based on the 'DESeq2' package normalization method.[87] Statistical analysis was done using the pair-wise comparisons between 21% oxygen vs 6% oxygen conditions within each genotype at each time point with DESeq2. PCA was performed using the Bioconductor package DEseq2 (version 1.10.1) in R software (version 3.1.3) based on variance-stabilized normalized read counts.[88] An OFDR (Overall False Discovery Rate) was calculated from the F-test's p-values for each gene by the Benjamini-Hochberg method. Only genes with OFDR < 0.05 were tested for the confirmation hypotheses. Enrichment analysis was performed with EnrichR.[78]

Lung sections image analysis

Regions of interest (ROIs) were manually defined using FIJI to exclude structures such as bronchi, terminal bronchioles, and blood vessels that may be misclassified as alveolar spaces. For each ROI, Raw Integrated Density was calculated by multiplying the mean intensity of the pixels by the area of the ROI. The area of alveoli was then expressed as a percentage of the total lung area. Trainable Weka Segmentation (WEKA)[76] was used to train the classifier manually on several datasets. Once trained, the algorithm was used to identify and isolate alveoli in the images. The percentage of alveoli area was calculated within the region of interest in the lung as previously described[89]

Lung Single cell RNA seq

Lung Single Cell Isolation

The whole lung of BHLKO and control AlbCRE male mice were collected at CT16 (3 biological replicates for each condition with total of 6 lungs). Cell dissociation was followed according to the Miltenyi Biotec lung dissociation kit protocol (#130-095-927). In short, the lungs were dissociated using enzymatic degradation followed by gentleMACS dissociation (#130-093-235) to obtain single cell suspension.

Single cell library preparation and sequencing using Chromium 10x genomics platform

Cells were counted and diluted to a final concentration in PBS supplemented with 0.04% BSA. Cellular suspension was loaded onto Next GEM Chip G at a concentration of 700-1200 cells/μL and then ran on a Chromium X instrument to generate GEM emulsion (10x Genomics). Single-cell 3' RNA-seq libraries were generated according to the manufacturer's protocol (10x Genomics Chromium Single Cell 3' Reagent Kit User Guide v3.1 Chemistry).

Single-cell 3' RNA-seq libraries were quantified using Next Library Quant Kit for Illumina (NEB) and high sensitivity D1000 TapeStation (Agilent). Libraries were pooled according to targeted cell number, aiming for ~20,000 reads per cell. Pooled libraries were sequenced on a NovaSeq 6000 instrument using an S1 100 cycles reagent kit (Illumina).

Single cell RNA-Sequencing Analysis

The Cell Ranger Single Cell Software Suite (v7.2.0) was used to perform post sequencing processing. The reads were aligned to the mouse transcriptome reference (mm10, Ensembl 93) with STAR[85] with including introns model. Raw read count tables were analyzed using the Seurat (v4.1.0)[90] standard pipeline on the R platform (v4.1.1). A total of 24,532 cells were sequenced and 25,332 genes counted. A median of 2,374 genes were detected per cell with a median of 5,670 UMI counts per cell. Cells with 200 > and < 8000 counts and < 25% mitochondrial reads were retained. Ribosomal genes denoted as [Rpsl], [Rplp] and [Rpsa] were removed. Following filtering, 22,741 cells remained; 10,706 which belonged to AlbCRE lungs and 12,035 belonging to BHLKO lungs. FindVariableGenes function was used to calculate the principal components. Cell clusters were identified using the shared nearest neighbor algorithm with a resolution parameter of 0.8, UMAP clusters were defined based on the first twenty principal components. To rule out potentially spurious results arising from variability across replicates, we adopted canonical correlation analysis to integrate the six samples using default parameters.[79] Scaling, PCA and UMAP were performed again using the first twenty principal components. FindAllMarkers function was used to identify genes significantly expressed in each cluster using Wilcoxon Rank Sum test (Data S6). FindMarkers function was used to identify differentially expressed genes between cell groups using Wilcoxon Rank Sum test (Data S7). 28 clusters of the 30 clusters were identified as specific cell types based off markers from the literature and SingleR[81] (Table S2).

Pseudobulking was carried out on each major cell type,[91] (Data S8). DESeq2[87] was used to identify significant gene expression changes (FDR < 0.05) within each major lung cell type cells. Pathway enrichment analysis was performed using ShinyGO (v8.0).[92] The Gene Ontology (GO) database was used. The top 10 pathways containing between 2 and 1000 genes were retained. For endothelial cells, stromal cells and alveolar macrophages, the expression from genes in clusters which corresponded to certain GO pathways were displayed as heatmaps across each of the biological replicates.

Blood Biochemistry Analysis

Blood serum biochemistry analyses (i.e., liver and kidney function tests, blood electrolytes, hemoglobin and hematocrit) were performed with American Medical Laboratories (AML).

Please cite this article in press as: Dandavate et al., Hepatic BMAL1 and HIF1α regulate a time-dependent hypoxic response and prevent hepatopulmonary-like syndrome, Cell Metabolism (2024), https://doi.org/10.1016/j.cmet.2024.07.003

Blood pH and gases measurements

Mixed arterial venous blood was collected in lithium-heparin coated tubes from the eye utilizing the retro-orbital bleeding method. The blood was added to the CG4+ cartridges (ABT-03P85-25) and blood pH and gases were measured with the iSTAT machine.

Histopathological examination

After sacrifice, livers and lungs were fixed in 4% paraformaldehyde (PFA) at 4°C overnight. Next day, 4% PFA was replaced by 1% PFA. The tissues were then embedded in paraffin, sectioned, and mounted on glass microscope slides. The sections were stained with hematoxylin and eosin and examined using light microscopy by two independent researchers who were blinded to the randomization scheme.

Baseline Echocardiography

AlbCRE and BHLKO mice were shaved on the chest and abdomen the day before the measurements using depilatory cream. To avoid a long exposure to isoflurane, which might influence the cardiovascular parameters, the experiment was performed on the following day.

The mice were anesthetized with isoflurane and set in a supine position on the mouse handling table. The ultrasound was performed using the MX550D transducer (Visual Sonics, with the cardiac settings). Parasternal long axis and short axis images of the left ventricle (LV) were acquired in B Mode. Next, short axis transaortic view, cross aortic views and 4 chamber images were recorded in B Mode. The mice were then allowed to wake up in a warmed cage and were returned to their home cages.

All the recordings were analyzed using the Vevo Lab (ver 5.8.1). The following parameters were extracted from parasternal long axis view of the LV in B mode: ejection fraction (EF), fractional shortening (FS) and Stroke Volume (SV). The Left atrium size was measured using the chambers view in B mode.

Measures of the left ventricular outflow tract diameter (d_{LVOT}) and right ventricular outflow tract diameter (d_{RVOT}) were made using respectively the parasternal long axis view of the LV and the short axis transaortic view. Measurement of the blood flow was made using colored and pulsed wave doppler in order to quantify the aortic and pulmonary flow, then aortic and pulmonary velocity time integral (Ao VTI and PAVTI, respectively) were calculated using the Vevo Lab software. The ratio Qp/Qs was calculated as such: $Qp/Qs= (\pi * (d_{RVOT}/2)^2 * PAVTI) / (\pi * (d_{LVOT}/2)^2 * AoVTI)$

Contrast enhanced echocardiography

Mice were shaved on the chest the day before the experiment using depilatory cream. Contrast enhanced echocardiography was performed using MX250 transducer and a Vevo 3100 system (Visual Sonics), with the Non Linear Contrast setting. The mice were anesthetized using isoflurane and an IV catheter (27G needle mounted on a silicone tube and then flushed 50 uL heparin) was implanted in the tail vein before imaging. The microbubble solution, the Vevo MicroMarker Non-Targeted Contrast Agent Kit for Tissue Enhancement, Perfusion and Microcirculation Applications (Visual Sonics) were purchased from Elsmed and diluted according to the Manufacturer instruction for cardiac imaging.

Mice were placed in supine position on the mouse handling table, with a nose cone to maintain anesthesia and their paws taped to the electrodes to monitor their heart and respiratory rate. Modified parasternal long axis images were acquired from the left ventricle (LV). The IV catheter was flushed with 100 uL of saline, then a volume of 50 uL of diluted (0.2 10^7 bubbles/uL) microbubbles was injected IV. The time and duration of the saline and of the microbubbles injections were marked in the recording. The images obtained were then analyzed using the Vevo Lab software (ver 5.8.1).

During analysis, the period between the injection of microbubble and their appearance in the left ventricle was measured as such: (frame number of apparition - frame visualization of the microbubbles in LV) x frame rate. The time from injection until the appearance of microbubbles in the LV was normalized to the animal's heart rate during this time window. The analysis was performed by an independent researcher who was blinded to the randomization scheme.

QUANTIFICATION AND STATISTICAL ANALYSIS

Statistics

All the statistical analyses were performed using R, and GraphPad prism (Version 9.1.0.221). Specific information on sample sizes, statistical significance, and variance measures is provided in the relevant figure legends.